Identifying Agglomeration Shadows: Long-Run Evidence from Ancient Ports

Richard Hornbeck, Guy Michaels, Ferdinand Rauch

Identifying Agglomeration Shadows: Long-Run Evidence from Ancient Ports

Abstract

We examine "agglomeration shadows" that emerge around large cities, which discourage some economic activities in nearby areas. Identifying agglomeration shadows is complicated, however, by endogenous city formation and \wave interference" that we show in simulations. We use the locations of ancient ports near the Mediterranean, which seeded modern cities, to estimate agglomeration shadows cast on nearby areas. We find that empirically, as in the simulations, detectable agglomeration shadows emerge for large cities around ancient ports. These patterns extend to modern city locations more generally, and illustrate how encouraging growth in particular places can discourage growth of nearby areas.

Richard Hornbeck
University of Chicago / IL / USA
Richard.Hornbeck@uchicagobooth.edu

Guy Michaels
London School of Economics and Political Science, London / United Kingdom
g.michaels@lse.ac.uk

Ferdinand Rauch
University of Heidelberg
ferdinand.rauch@awi.uni-heidelberg.de

Cities benefit from agglomeration spillovers that raise productivity but may also cast "agglomeration shadows" that discourage some economic activities in surrounding areas. City growth can increase population density in nearby areas as cities expand outward from their historical centers, but the broader economic gains may be tempered if nearby areas are relegated to second-tier status in an urban hierarchy. Given sizeable urban-rural differences in productivity, wages, and housing costs, spatial inequality is amplified if encouraging city growth in particular areas discourages city growth in nearby areas.

There have long been models of urban hierarchies (Jefferson, 1939), with larger cities spaced out and interspersed with smaller cities (Christaller, 1933; Lösch, 1940). The New Economic Geography literature modeled how such a system of cities can emerge (Fujita and Krugman, 1995; Fujita, Krugman, and Mori, 1999; Fujita, Krugman, and Venables, 1999). Fujita, Krugman, and Mori (1999) start with a central city, in which firms cluster to benefit from agglomeration forces and increasing returns to scale. As population grows, new cities emerge to serve an agricultural hinterland. While some small cities may emerge closer to the central city, larger cities only develop further away because they face strong competition from the central city without benefiting from its agglomeration forces. The central city thereby casts a shadow, discouraging some economic activity nearby.

While agglomeration shadows may be important in shaping the spatial distribution of economic activity, it is challenging to identify these shadows for two main reasons. First, cities grow in particular places, endogenously, in ways that both reflect and influence the potential growth of nearby cities. In empirical settings, there is generally not an exogenously-fixed starting central city from which to consider the causal impacts on surrounding areas. Second, we use the model from Fujita, Krugman, and Mori (1999) to show in simulations that a form of "wave interference" emerges when averaging across the surroundings of many central cities. This wave interference arises because small differences across urban networks make their spatial patterns asynchronous, which can obscure the alternating empty spaces and cities (especially for smaller cities that are often not spaced as far apart).

To overcome the reflective endogeneity in city growth, we study shadows cast by cities "seeded" at 4,263 ancient port locations that surrounded the Mediterranean, Black Sea, Red Sea, and nearby coastal areas. We find that ancient port locations are more likely to have grown modern cities than geographically-similar locations, even when there are no longer natural harbors in the ancient port locations to precisely pin down modern city locations. We then estimate the probability that modern cities emerged near the ancient port locations, which reflects the presence of agglomeration shadows from cities seeded at those ancient port locations. The identifying assumption is that ancient ports are not otherwise associated with city formation in surrounding areas, aside from encouraging city growth in that port location.

1

Ancient ports may even have direct effects on modern activity in those port locations, but our focus is identifying impacts on surrounding areas.

We overcome the challenge of "wave interference" in two ways. First, we focus on agglomeration shadows in large city locations, which are less obscured by wave interference in model simulations because larger cities are rarer. Second, we contrast places where a natural harbor has survived, pinning down economic activity more precisely to the ancient port locations, to locations where a harbor has disappeared.

The empirical analysis uses population data for 1km-by-1km grid cells (CIESIN, 2018), which cover 2.3 million square km within 200km of an ancient port and within 50km of the coast. We examine the spatial distribution of population density in grid cells around ancient port locations, controlling for grid cells' distance to the coast and nearest river, as well as other "first nature" geographic features that may affect city formation (e.g., ruggedness, temperature, precipitation). We also report estimates that control for endogenous features of the ancient era, such as distance to Roman roads or proximity to ancient cities.

We first estimate that grid cells with ancient ports have higher modern population density, on average, and are more likely to have become urban areas or cities than geographically similar grid cells. Grid cells with ancient ports are 12 percentage points more likely to have urban population density (ln density > 6) and 1.7 percentage points more likely to have city population density (ln density > 9), whereas 7.1% of sample grid cells have urban density and 0.2% have city density.

We estimate that average population density declines monotonically in distance from the ancient port locations. Ancient ports' impact on log population density extends beyond city boundaries and at 50km is roughly one-fourth the impact at the ancient port location. These impacts are similar – smaller, but still substantial – around ancient port locations that have since lost their natural harbor. These estimates suggest path dependence in economic activity, not only in particular locations with obsolete geographic advantages but also in ways that extend to surrounding locations.[1]

We then explore the existence of "agglomeration shadows" around these ancient port locations, which are detectable in our simulations at higher thresholds of population density. We find that urban activity (ln density > 6) declines monotonically in distance from the ancient ports with harbors, whereas city activity (ln density > 9) declines more quickly out to 20km and then increases up to 40km. This estimated agglomeration shadow in city formation, at 10-30km from ancient port locations, is similar to the distance of a typical

---

[1]We focus on the presence of a natural harbor in modern satellite images, setting aside the existence of modern human-made harbors, which are potentially endogenous to local economic demand. Our estimates are also not sensitive to omitting a small number of cases with known ancient investments in open-water ports.

day's travel for pack animals or carts in the ancient world (Scheidel, 2015).

Consistent with the model's prediction on agglomeration shadows, the likelihood of finding city density follows a distinctive wave pattern around the locations of ancient ports whose natural harbors survived and pinned down the location of their seeded city. Agglomeration shadows are more obscured around ancient ports that lost their harbors, for which there is more wave interference. In contrast to the wave pattern for city densities, we observe mono-centric declines in urban activity that are similar to classic models of monocentric cities (Alonso, 1964; Mills, 1967; Muth, 1969), but are also consistent with "wave interference" from a combination of positive and negative spatial impacts at different distances.

The agglomeration shadows in city activity appear to reflect general city-to-city crowd-out, rather than direct competition between ports themselves. We estimate that ancient port locations are not more likely to have modern port structures when nearby ancient port locations have lost their harbors (and thereby have less port activity). By contrast, these ancient port locations do appear to be in competition for more general economic activity: ancient port locations have higher population density, urban activity, and city activity when nearby ancient port locations have lost their harbors (and thereby have less general economic activity).

We conclude by examining the spatial distribution of all modern cities in our sample region, where we find indications of agglomeration shadows more generally. We calculate the distance from each modern city to the nearest modern city (from GHS-UCDB 2019 data), and we plot the cumulative distribution function (CDF) of distances. We compare this observed CDF to the distribution of CDFs for minimum distances between randomly located cities, where these random locations are selected in simulations using probability weights to reflect geographic characteristics that predict city formation. Consistent with the existence of agglomeration shadows in the modern spatial equilibrium, we observe fewer large cities (> 500,000 people) whose nearest large city is within 40km. We then observe more large cities than expected from 40km to 60km.

Our main contribution is to use the historical influence of ancient port locations to demonstrate causal negative "agglomeration shadows" that are consistent with longstanding theory (Christaller, 1933; Lösch, 1940; Fujita, Krugman, and Mori, 1999), which echoes the use of establishment openings to demonstrate causal positive "agglomeration spillovers" (Greenstone, Hornbeck, and Moretti, 2010; Bloom et al., 2019; Giroud et al., 2021), which also follows a long intellectual tradition (Marshall, 1890; Ellison and Glaeser, 1997; Glaeser and Gottlieb, 2009). Our estimates draw on an empirical literature documenting local path dependence (Bleakley and Lin, 2012; Michaels and Rauch, 2018), and we extend this literature to consider path dependence in spatial relationships beyond those locations. We

3

show that these resulting agglomeration shadows are obscured by a pattern of "wave inter-ference," which we document using simulations that extend the model in Fujita, Krugman, and Mori (1999). Identifying agglomeration shadows is also complicated by classic challenges to causal inferences from endogenous city formation. The locations of ancient ports, and variation in the survival of natural harbors, provide empirical traction to estimate the presence of agglomeration shadows. Our main departures from existing empirical research on agglomeration shadows are to (1) use historical determinants of starting city locations for identification, and (2) connect our empirical tests more closely to theoretical predictions from simulations based on Fujita, Krugman, and Mori (1999).

When cities cast shadows, local economic growth can discourage some nearby activities and encourage them further away. The existence of agglomeration shadows implies broader impacts of place-based policies. Similar types of agglomeration shadows may also arise in access to specific services at different locations, such as spatial differences in healthcare access (Finkelstein, Gentzkow, and Williams, 2021; Dingel et al., 2023) or food deserts (Cummins and Macintyre, 2002). We focus on identifying how major cities affect nearby places, using the locations of ancient ports to gain empirical traction in identifying forces long hypothesized but relatively overlooked in the recent focus on identifying positive agglomeration spillovers.

Section I discusses related literature, simulations of agglomeration shadow forces in the model of Fujita, Krugman, and Mori (1999), and implications for empirical analysis of agglomeration shadows using ancient ports. Section II introduces the data, with more details in Appendix A, and Section III describes our estimating equations. Section IV reports our estimates using ancient port locations, and Section V analyzes agglomeration shadows among modern cities more generally. Section VI concludes.

I   Related Literature and Model Simulations

I.A   Agglomeration Spillovers and Agglomeration Shadows

Economic activity is spatially concentrated, partly because of natural advantages to particular locations but also because proximity to other economic activity increases productivity due to "agglomeration spillovers." Manufacturing industries, for example, are more spatially concentrated than can be explained by natural advantages or random chance (Ellison and Glaeser, 1997, 1999; Duranton and Overman, 2005; Ellison, Glaeser, and Kerr, 2010; Mori and Smith, 2015). Indeed, the opening of large manufacturing establishments increases the productivity of nearby incumbent establishments (Greenstone, Hornbeck, and Moretti, 2010). These direct productivity benefits do not extend to further geographic areas but do spread to further establishments owned by those incumbent firms (Giroud et al., 2021) in part through changes in management practices (Bloom et al., 2019).

Cities are not just points in space, representing central business districts where these positive agglomeration spillovers may be strongest. In classic models of "monocentric cities," population density and land prices are highest at the city center and decrease in distance from this center (von Thünen, 1826; Alonso, 1964; Mills, 1967; Muth, 1969; Duranton and Puga, 2004). This empirical pattern is common, though there are deviations and extended models consider "polycentric cities" (Ahlfeldt and Wendland, 2013; Ahlfeldt et al., 2015). The broader economy then includes a distribution of cities of different sizes (Henderson, 1974; Gabaix, 1999), with a greater range of economic activities in larger cities (Davis and Dingel, 2020).

Strong agglomeration forces raise the prospect of "agglomeration shadows," whereby concentrated economic activity in cities actively discourages some nearby economic activities. In early models of urban hierarchies (Christaller, 1933; Lösch, 1940), a featureless plain is evenly populated by farmers and is served by a hexagonal lattice of "central places" in a hierarchy: larger cities are spaced far apart, producing a broad range of urban goods and services, and smaller cities fill-in intermediate areas to offer a narrower range of goods and services.

The tension between congestion and dispersion forces is captured by models in the New Economic Geography literature, which provide micro-foundations that rationalize the emergence of urban hierarchies through a decentralized process (e.g., Fujita and Krugman 1995; Fujita, Krugman, and Mori 1999; Fujita, Krugman, and Venables 1999; Fujita and Mori 2005; Mori et al. 2023).[2] These models predict that cities create agglomeration shadows, discouraging city formation in surrounding areas, but the length of these shadows varies by cities' sizes and the diversity of their economic activity. Large cities are less likely to form near other large cities in these models, but smaller cities may still form closer to large cities.

I.B   Agglomeration Shadow Appearance in Simulations

We build on the model of Fujita, Krugman, and Mori (1999), "FKM model," to simulate how agglomeration shadows appear when estimating average impacts across many geographic areas.

The FKM model describes a one-dimensional economy, with a fixed initial city and other locations indexed by distance r from that initial city. There are two sectors in the model, "manufacturing" and "agriculture." Within manufacturing, there are three industries that each produce a continuum of differentiated goods using labor and production technology with increasing returns to scale. Manufacturing concentrates in cities, whose number and location are determined endogenously. The agricultural sector produces one homogeneous

---

[2]See also a literature on regional variation in industry activity from the Home Market Effect (Helpman and Krugman, 1985; Matsuyama, 2017; Costinot et al., 2019).

good, using labor and land in rural areas, with constant returns to scale production.[3] Goods are traded with iceberg transportation costs. Consumers have Cobb-Douglas preferences over agricultural goods and composite indices of manufactured goods in each industry, with constant elasticity of substitution (CES) preferences over varieties of manufactured goods. Within manufacturing, industry 1 has the highest elasticity of substitution across varieties, followed by industry 2 and then industry 3, such that consumers are most willing to incur transportation costs for industry 3 goods. Labor is supplied by consumers, who are fully mobile across locations and sectors, and land is of homogeneous quality.

The model has multiple equilibria, but Fujita, Krugman, and Mori (1999) explore the following scenario. When aggregate population N is small, all manufacturing occurs in the fixed initial city. As N increases, the agricultural frontier expands. Once N increases sufficiently, there is enough market potential to produce some manufactured goods away from the central city, and a "third-order" city emerges with manufacturing production only in industry 1. As N grows further, the agricultural frontier keeps expanding and additional cities emerge: more single-industry "third-order" cities, and a small number of two-industry "second-order" cities that are further apart from the central city and each other. The initial city is the only "first-order" city, by assumption, with all three manufacturing industries.

In simulations, we explore how this model generates average impacts on city formation around fixed initial starting locations in independent economies of different sizes. We assume a range of values for aggregate population N that follows FKM, and we graph the share of cases in which cities form at each distance r.[4] The model is symmetrical around zero, and like FKM we show locations that are on the positive side, distance r from the fixed starting location.

Figure 1 shows the averaged spatial distribution of cities. There is always a city at the origin, by assumption, and some distances often have a city, while others rarely do (Panel A). Panel B shows the averaged spatial distribution of "large cities," which are second-order or first-order cities with two or three manufacturing industries. These second-order and first-order cities typically have larger populations in the model, on average, though population density is not well-defined in the model because cities do not take up space.

For each aggregate level of population, the FKM model determines city locations relative to the fixed starting point where the central city emerges. We also consider the possibility

---

[3]"Manufacturing" and "agriculture" could reflect a range of goods and services, where the important feature of the model is that "manufacturing" is done in cities with increasing returns to scale and "agriculture" is done across places with constant returns to scale.

[4]We use the 16 distinct values for aggregate population N reported in Figure 7 of Fujita, Krugman, and Mori (1999). Where there are bifurcations, we choose the side of the bifurcation associated with higher population.

that the central city may not emerge exactly at a fixed point (e.g., an ancient port). Instead, we allow for the initial city to form near the fixed starting point, at a location drawn randomly from a normal distribution centered on the fixed starting point with a σ standard deviation. We simulate the model 2,000 times, for each level of aggregate population, and graph the share of cases in which cities form at each distance r, only on the positive side from the fixed starting point.

Figure 2 shows the share of cases in which cities form at each location, with increasing spatial noise. There are visible waves in the probability of any city when allowing for small spatial noise (Panel A), and further waves in large city locations (Panel B). Allowing for more spatial noise, the peaks and valleys in small city locations overlap and this "wave interference" generates a monotonic decline in the frequency of any city in distance from the origin (Panel C).

This notion of "wave interference" relates to asynchronous waves offsetting each other, which here arises from "high-frequency" probability density functions for city locations that obscure each other's signal. The locations of large cities are less subject to this wave interference because of their lower frequency, corresponding to larger underlying gaps. Thus, as we move away from the origin, the probability of finding a large city decreases and then increases (Panel D), reflecting the still-detectable shadow cast by the largest city. But as spatial noise increases further, there are more monotonic declines for both all cities and large cities (Panels E and F).

Figure 3 overlays the spatial distributions of cities, with more or less spatial noise, for all cities (Panel A) and large cities (Panel B). Panels C and D report the differences in these lines, with a dip and upward movement in large city formation (Panel D) and a smoother decline and leveling out in all city formation (Panel C). Appendix Figures A.1, A.2, and A.3 report similar figures for the probability that particular distances exceed certain population density thresholds, separating distances into sized grid cells and normalizing the density thresholds based on the grid cell size and aggregate population.

These simulations suggest how agglomeration shadows appear when averaging impacts on nearby areas from multiple starting cities, each "seeded" at a separate location (e.g., an ancient port). Agglomeration shadows are most clearly visible for large densely-populated cities when seeds pin down the precise location of starting cities. Due to wave interference, these shadows become less visible as spatial noise in the starting city location increases, particularly shadows for smaller urban areas that are closer together. We then expect agglomeration shadows to be more visible for large cities than smaller cities and when starting city locations are precisely pinned down (e.g., when the natural harbor survived) than when there is more spatial noise in starting city locations (e.g., when the natural harbor disap-

7

peared).

We expect a similar form of wave interference from spatial noise due to heterogeneity in the model parameters, which presumably vary across time periods and regions where urban hierarchies emerge. For example, higher or lower transportation costs would shrink or expand the wave pattern in city locations and create wave interference when averaging across those areas. Cities also take up space, and variation in this space will also create a wave pattern resulting in interference. Rather than simulate each of these cases, we note that adding noise to the starting city location is analytically convenient, maintaining the same solution as FKM, and also corresponds to cases in which the starting city location is pinned down more or less precisely at an ancient port location, depending on whether the natural harbor survived.

The FKM model provides one underlying micro structure that generates agglomeration shadows, but different micro structures could also generate the empirical occurrence of agglomeration shadows and wave interference obscuring small gaps between smaller cities. FKM focuses on local increasing returns to scale in manufacturing production, which generates agglomeration shadows because nearby (shadowed) places can import goods and do not benefit from local returns to scale. A similar mechanism can also apply in the case of local knowledge spillovers in manufacturing, and different micro structures can have different welfare implications. Rather than focusing on parameter estimation, we use the simulations to show how agglomeration shadows may appear in data.

I.C   Estimating Agglomeration Shadows

The FKM model illustrates endogenous city formation, but takes an initial starting city as given, which highlights a central empirical challenge: finding exogenous "fixed" starting locations for local urban networks. A city may form in a particular place when surrounding areas are unsuitable, rather than the city itself discouraging nearby city formation. Related empirical literature takes city locations as given and estimates how population growth varies with distance to cities (Ali et al., 2009; Tervo, 2010; Cuberes, Desmet, and Rappaport, 2021; Beltrán Tapia, Díez-Minguela, and Martinez-Galarraga, 2021).

We look to estimate how an urban hierarchy emerges, in which cities affect each other's development over a long time horizon. Indeed, Bosker and Buringh (2017) find that, from 800-1800, new European cities were less likely to form within 20km of existing cities and more likely to form 20-100km from existing cities. European cities were also more likely to form in areas with transportation network advantages, which relates to a literature that explores how economic activity in some places can be affected positively and negatively by connections to other places (Redding and Sturm, 2008; Faber, 2014; Donaldson and Hornbeck, 2016;

Barsanetti, 2023; Hornbeck and Rotemberg, 2024).

We use ancient ports that encouraged city growth in particular places, due to highly-local coastline characteristics, to estimate impacts on surrounding areas. This is an advantage of ancient ports, in contrast to using all ancient cities whose locations reflect the economic suitability of their surrounding areas to a greater extent. Another useful feature of ancient port locations is that sufficient time has passed for some of them to grow cities, and for the resulting cities to become locked into place (as in Michaels and Rauch 2018), such that we can then explore impacts on surrounding areas.

Our empirical strategy draws on the literature on "pointwise" path dependence, which highlights that city locations can be influenced by geographic features that had historical economic relevance. Bleakley and Lin (2012) estimate that "portage sites," where waterway transportation required carrying goods around rapids, became places with persistently higher population density in the United States.[5] The theory of Fujita and Mori (1996) explores how cities may form in port locations and continue to thrive after ports themselves become less central to their economic activities. We use the path dependence of activity at ancient port locations to explore how these sites influenced the spatial distribution of population in surrounding areas and identify agglomeration shadows.

An advantage of analyzing ancient port locations, which were "seeds" for later cities, is that the local geographic feature that gave rise to an ancient port is plausibly not directly associated with modern outcomes in places 10-50km away. Even for the ancient port locations themselves, the large majority of these locations have no commercial shipping presence today and many have no apparent port structures in satellite images. Even when the natural harbor survived, maritime activities are not as central to the modern economy. Ducruet et al. (2024) find zero impact on local population from even large-scale commercial ports in the modern era, though containerization raised population around some ports relative to other ports (Brooks, Gendron-Carrier, and Rua, 2021). Port structures in surrounding locations may compete with each other but can also be complementary; in our context, we do not find evidence of local spatial crowd-out in modern port construction among our ancient port locations.

A related literature analyzes the historical development and evolution of cross-city trading networks (Greif, 1993; Abulafia, 2011; Barjamovic et al., 2019; Flückiger et al., 2021; Bakker et al., 2021; Maurer and Rauch, 2022), whereas we focus on the local economic ge-

---

[5]Bleakley and Lin (2012) also show the emergence of "sister cities" at river mouths downriver from their corresponding portage sites, though we control for distance to the coast and river mouths that have direct geographic advantages. Roman roads also generate higher local modern economic activity (Dalgaard et al., 2022; de Benedictis, Licio, and Pinna, 2023), with long-run increases in economic activity also around the Inca Road (Franco, Galiani, and Lavado, 2021) and Silk Road (Ahmad and Chicoine, 2021).

ography around ancient port locations and the cities they seeded. We examine ancient port locations, rather than ancient cities, because even those ancient city locations may reflect nearby areas' characteristics and an already-developing urban hierarchy. Ancient ports reflect the highly-local geographic availability of natural harbors in the ancient era, whereas ancient transportation infrastructure follows desirable and feasible routes. The ancient port structures are long gone, and even the natural harbors are gone in a fifth of cases, and we verify that our estimates are robust to controlling for proximity to ancient roads or larger ancient cities.

II Data Construction

II.A Ancient Port Locations

We start with a database of ancient port locations, assembled by de Graauw (2019), which has precise geographic coordinates of ports mentioned in ancient texts and histories. The full database includes 4,561 ancient ports across Western and Southern Europe, North Africa, and Western Asia. We exclude ports more than 50km from the modern coast and those in remote areas with less complete coverage, which leaves 4,263 ancient ports (Figure 4).

We do not observe other characteristics in the ancient era for these port locations, but we expect these locations had natural harbors following exchanges with de Graauw.[6] These ancient ports are defined as places that served seafarers, rather than just local fishing. Ancient seafarers had more need for frequent stops and safe harbors, in contrast to the modern era in which fewer ports are needed.

For each ancient port location, we use Google Earth images to hand-code additional data for the modern period, including whether these locations have a natural harbor. We focus on the presence of natural harbors, setting aside the visible influence of human-made harbor protections, and our use of "harbor" refers to "natural harbor" unless otherwise specified. For ancient port locations, 80% retained their natural harbor (Figure 4, Panel B) and 20% lost their natural harbor (Figure 4, Panel C). We also collect data on the presence of modern port structures: 46% have any port structures and 6% have commercial port structures.

The loss of natural harbors was fairly common and widespread, occurring throughout the sample region. Typical reasons for the loss of a natural harbor are long-run natural processes of silting and coastal drift, along with rarer sinking and land rise. Harbor loss occurred even near major ancient cities, such as Rome (Portus, Ostia Antica), Alexandria (Thonis-Heracleion), Leptis Magna, and Caesarea Maritima, as people were unable to resist the natural processes causing harbor loss for long periods.

---

[6]There are 22 open-water ancient ports, which had more human-made support and were less reliant on a natural harbor, which we exclude in robustness checks.

II.B Population Data

We use population data for 1km-by-1km grid cells in 2015 from GPWv4 (CIESIN, 2018). GPWv4 uses the areal weighting of detailed population data to assign all grid cells a population in 2015, also drawing on data from other years and estimated growth rates.

Our sample covers 2.3 million grid cells within 50km of the coast and within 200km of their nearest ancient port. For context, in the ancient era, a typical day's travel for pack animals or carts was 12-30km (Scheidel, 2015), and medieval royal itineraries suggest that a day's land travel speed was stable at around 40km per day for many centuries (Hall, 2023). 4,263 grid cells have at least one ancient port, and Appendix Figure A.4 shows the number of sample grid cells by distance to their nearest ancient port.

These data provide detailed geographic variation in "city" and "urban" activity. We define "city" activity as log population density above 9, or roughly 8,000 people per square km. We define "urban" activity as log population density above 6, or roughly 400 people per square km. We also report impacts on average log population density.[7]

For robustness analysis, we use other measures of local economic activity. We use grid-cell population data for 2000, or GRUMP data (CIESIN, 2011), based on an earlier version of the GPW database that reflects a less-developed data model.[8] We also check robustness to using population data from the Global Human Settlement Layer or GHSL (Schiavina, Freire, and MacManus, 2019).[9] Our later simulation exercises also use city locations from GHSL's Urban Centre Database (Florczyk et al., 2019), which provides city centroid coordinates and geographic area along with total population. It would be useful to have population data through the intermediate historical periods, between the ancient era and present-day, but data are not available at a fine enough spatial resolution to cover economic activity comprehensively in and around the ancient port locations.

II.C Geographic Characteristics and Other Data

Our empirical analysis allows for spatial variation in geographic determinants of cities and economic activity, in contrast to the motivating theoretical framework that assumes a featureless plain. We look to control for "first nature" location characteristics.

Along with restricting our analysis to areas within 50km of the coast, we measure grid

---

[7]Throughout the paper, "log" refers to the natural logarithm.

[8]The GRUMP dataset uses an older version of GPW data as an input (GPWv3) and then reallocates the population data according to urban-rural distributions within administrative units based on night lights data and settlement population counts. GPWv4 instead uses higher-quality population inputs to construct a grid, with coverage and granularity improvements such that the number of input administrative units increases five-fold. As a result, GPWv4 has nonzero population densities at many more locations.

[9]GHSL re-weights and adjusts the same inputs as GPWv4 with a focus on "built-up" areas and settlements. Because we are interested in the lack of settlement density as well as its presence, which can be sensitive to GHSL decisions about city boundaries, we use the GPWv4 model in our main specifications.

cells' distance to the coast, distance to major rivers, and latitude/longitude. We also include terrain ruggedness, based on the standard deviation of elevations within the grid cell, which influenced locations of economic activity in the region (Nunn and Puga, 2012; Accetturo, Cascarano, and de Blasio, 2019). Our baseline controls also include grid cells' average temperature and precipitation in both January and July.

For robustness analysis, we use a variety of other geographic characteristics. We measure agricultural suitability from the FAO-GAEZ database for 6 crops: potatoes, cowpeas, olives, chickpeas, wheat, and barley. We also measure whether a grid cell is in a desert. We define grid cells' country or, given the endogenous formation of country boundaries, group cells into 2-degree square fixed effects. We measure whether grid cells are on an island, and sometimes exclude cells on islands smaller than 2,500km^2.

We also use some data from the ancient era. These include data on locations of the most important ancient cities and towns from the Barrington Atlas (Talbert, 2000; Hanson, 2016): the 14 most important ancient cities in our region ("Category 1"); the 160 next most important ("Category 2"); and 813 less important cities and towns ("Category 3"). We compare the local impacts of ancient ports to these ancient cities, and sometimes exclude areas within 20km of Category 1 ancient cities. We also measure distance to the nearest Roman road, as a potential control variable though endogenous to ancient development.

Appendix A provides additional details on the data sources and our database construction.

III   Main Estimating Equations

We start by estimating the local impacts of ancient ports on modern outcomes in grid cell i:

$$(1) \qquad Y_i = \beta Port_i + \theta \mathbf{X}_i + \varepsilon_i.$$

Outcomes Y_i include log population density and indicators for log population density exceeding 6 (urban activity) or 9 (city activity). The coefficient β reports differences for grid cells with an ancient port, compared to other grid cells with similar geographic characteristics ($\mathbf{X_i}$). Our baseline controls included in $\mathbf{X_i}$ are: log distance to the coast; log distance to the nearest major river; latitude; longitude; terrain ruggedness; and average temperature and precipitation in both January and July.

Our main specification extends equation (1), estimating impacts by distance to nearest ancient ports:

$$(2) \qquad \begin{aligned} Y_i &= \sum_{d=0km}^{50km} \beta_d^H NearestPort_i^{Harbor} \in [d, d+1) \\ &+ \sum_{d=0km}^{50km} \beta_d^{NH} NearestPort_i^{NoHarbor} \in [d, d+1) + \theta \mathbf{X}_i + \varepsilon_i. \end{aligned}$$

The coefficients β_d^H report impacts by distance to the nearest ancient port with a surviving natural harbor, which is likelier to pin down city locations to ancient port locations. The coefficients β_d^{NH} report impacts by distance to the nearest ancient port with no surviving natural harbor.[10] More distant ports could also matter, in principle, but the motivating theoretical framework has clearest predictions for distance from a particular fixed starting location. We jointly estimate these distance bins, for each type of ancient port, because proximity to an ancient port without a harbor is correlated with proximity to an ancient port with a harbor. We include all baseline controls from equation (1).

We graph these non-parametric estimates, by distance bin. We also report the fitted relationship with log distance to nearest ancient port, along with estimated deviations between the non-parametric estimates and this fitted relationship.

Our baseline specifications report standard errors clustered by 8km-by-8km groups, which reflects typical large-city boundaries in our sample region.[11] We allow for spatial correlation across grid cells because cities take up space, whereby one large city may generate measured "city activity" across nearby cells. The statistical inference is robust to different adjustments for correlated outcomes across nearby cells.[12]

IV Population Growth and Agglomeration Shadows around Ancient Ports

IV.A Main Estimates

Table 1 reports higher modern population density in grid cells with ancient ports, compared to otherwise geographically-similar grid cells, from estimating equation (1). Grid cells with an ancient port are 1.7 percentage points more likely to have city population density (Panel A, Column 3), which is large relative to the sample mean probability of 0.2 percentage points. Ancient port grid cells are also 12 percentage points more likely to have urban population density (Column 2), compared to a sample mean probability of 7.1 percentage points. Average population density is also 60% higher in ancient port grid cells (Column 1). The impacts of ancient ports are more subtle than the impacts of ancient cities themselves (Panel B), which are potentially more related to the suitability of surrounding areas for city formation, but there is a sufficiently large number of ancient ports for their effects to be

---

[10]We mostly compare these coefficients to each other, but their absolute value is estimated relative to the omitted distance categories that are >50km for each port type.

[11]We cluster by 1/12-degree-by-1/12-degree groups, which are roughly 8km-by-8km squares in the middle of our sample region. By comparison, 8km is the median city diameter for cities in our sample region (from GHSL 2019).

[12]We also report standard errors two-way clustered by offset 8km-by-8km groups, shifted by 4km North-South and East-West to allow for spatial correlation across the 8km-by-8km groups, or clustered by 25km-by-25km groups. We report Conley standard errors, which adjust for spatial correlation that declines linearly up to a distance cutoff of 4km or 8km, which are computationally intensive for the entire sample but similar to the group-clustered standard errors.

precisely estimated.

Figure 5 shows impacts on average population density by distance to ancient ports, from estimating equation (2). The impacts on average population density decline in distance to ancient ports and remain positive at 50km, relative to further grid cells. The nearby impacts are larger for ancient ports that retained their natural harbor (blue circles), but still substantial for ancient ports that have lost their natural harbor (red circles).

Figure 6 shows impacts on urban density and city density, by distance to ancient ports, which correspond to the simulated appearance of agglomeration shadows in Section I. There is greater likelihood of city density at the ancient port, or within a few kilometers, when the ancient port location has retained its natural harbor (Panel B, blue circles). This probability of city density declines quickly in distance, however, and is lowest around 20km from the ancient port before increasing moderately out to a distance of around 40km. By contrast, when the ancient port location has lost its natural harbor, there is more spatial noise in that starting city location out to 20km before the probability of city density declines (Panel B, red circles). Panel A reports corresponding estimates for urban density, which show more monotonic and continued declines in urban activity by distance to ancient ports.

Panels C and D of Figure 6 report the differences in these estimates ($\beta_d^H - \beta_d^{NH}$), which correspond to the simulated differences in Panels C and D of Figure 3. In our data, as in the simulations based on FKM, there is a distinctive relative dip in the likelihood of city density at intermediate distances (Panel D) and a more flattened relative decline in urban activity (Panel C).

Figure 7 adds a fitted log relationship to the estimates from Figure 6, Panels A and B. The decline in urban activity is roughly logarithmic in distance to the ancient ports (Panel A), whereas the dip in city activity (Panel B) at intermediate distances is more distinctive from a smooth logarithmic decay in distance. The decline in city density is more rapid from 0-20km from the ancient port location, and then this pattern reverses from 20-40km. Panels C and D of Figure 7 report the deviation in the estimates from the fitted log relationship, by distance. When the ancient port more precisely pins down a starting city in that location (i.e., when that ancient port has retained its natural harbor), there is a distinctive decline in the likelihood of city activity at intermediate distances. Once at a further distance, however, there is again a greater likelihood of a city emerging relative to the fitted log relationship.

Table 2 reports a few numbers from Figures 6 and 7, Panel D. From Panel D of Figure 6, the differences in city probability are -0.42 percentage points at 20km and 0.12 percentage points at 40km, as compared to the sample mean probability of 0.20 percentage points (Table 2, Panel A, Columns 1 and 2). This difference of 0.54 percentage points is statistically significant (Column 3). From Panel D of Figure 7, the deviation from log fit is -0.25

14

percentage points at 20km and 0.16 percentage points at 40km (Table 2, Panel B).

Cities "seeded" at ancient port locations appear to generate agglomeration shadows, discouraging the formation of cities at intermediate distances. The length of this agglomeration shadow is similar to a typical day's travel of 12-30km for pack animals or carts in the ancient era (Scheidel, 2015). Cities were more likely to form further away, where there was less direct competition with city activity at the ancient port location.

Our analysis focuses on the appearance of agglomeration shadows in city formation within a 50km-radius catchment zone. In principle, similar underlying economic forces could influence highly-tradable economic activities at much further distances – and in ways that interact across multiple starting cities – but modeling and estimating such interactions across further distances is beyond the scope of our analysis.

IV.B Robustness

The appearance of agglomeration shadows, around cities seeded at ancient ports, is not sensitive to adjusting for some other sources of spatial variation in economic activity. We explore several types of adjustments to our baseline analysis: controlling for additional grid cell characteristics; sample restrictions; alternative measures of city locations; and adjusted inference for spatial correlation.

One concern would be if grid cells within 10-30km of ancient ports happen to be particularly less suitable for city formation than grid cells closer to (or further from) ancient ports. Our baseline specification controls for log distance to the coast; log distance to the nearest major river; latitude; longitude; terrain ruggedness; and average temperature and precipitation in both January and July. Appendix Figure A.5 includes additional controls for geographic characteristics of the 1km-by-1km grid cells: six crop-specific measures of agricultural suitability (wheat, barley, chickpeas, cowpeas, olives, potatoes);[13]; suitability of nearby waters for fishing;[14] log distance to the mouth of a river; indicators for being within 2km, 5km, and 10km of the coast, a river, and the mouth of a river; elevation; and indicators for being in a desert or on an island. Appendix Figure A.6 excludes all grid cells on islands smaller than 2,500 square kilometers (5% of all grid cells). Appendix Figure A.7 reports similar estimates when excluding 216 locations that de Graauw is less certain of their use as ancient ports.

We also report estimates that adjust for other features of the ancient economy. Appendix Figure A.8 includes controls for grid cells' log distance to the nearest Roman road, along with

---

[13]From FAO GAEZ's historical agro-climatic crop suitability data, assuming low inputs (FAO, 2012). The first five crops were important in the ancient era, among those with available crop-specific data, whereas potatoes were influential later (Nunn and Qian, 2011).

[14]Following Dalgaard, Knudsen, and Selaya (2020), we use the average suitability of waters within 100km for 15 common fish species, with data from Aquamaps (2019).

log distance to 14 important ancient cities (Barrington 1 sites), though these already reflect responses to the early formation of a geographic urban hierarchy. Appendix Figure A.9 excludes grid cells within 20km of 22 ancient open-water ports, which reflect known human-made investment in artificial harbor breakwaters, and Appendix Figure A.10 excludes grid cells within 20km of the Barrington 1 sites.

Our sample covers a broad geographic area, but our estimates are not sensitive to adjusting for more regional variation in economic activity. Appendix Figure A.11 includes controls for 2-degree by 2-degree fixed effects in cells' latitude and longitude, and Appendix Figure A.12 includes country fixed effects.

Our main analysis classifies "city activity" and "urban activity" as grid cells with log population density greater than 9 and 6, respectively. Appendix Figures A.13 and A.14 show the emergence of agglomeration shadows as the population density threshold increases from 5 to 10. We use population data from 2015, using version 4 of the GPW model, but estimates are similar using population data from 2000 from an earlier version of the model (Appendix Figure A.15). Estimates are also similar in Appendix Figure A.16 using population data from 2015 from the GHSL-POP model (Schiavina, Freire, and MacManus, 2019). Appendix Figure A.17 reports estimates using city locations from GHSL (Florczyk et al., 2019), where the outcome is being within the radius of a city of population over 500k.

We allow for spatial correlation across grid cells, as the median-size city in our sample region has a radius of 4km and so one realization of city formation can be jointly reflected in nearby cells. Our baseline inference clusters in 1/12-degree by 1/12-degree groups, or roughly 8km by 8km squares in the middle of our sample region. Appendix Figure A.18 reports similar standard errors when two-way clustering with offset groups, shifted by 1/24 of a degree, which relaxes the assumption that grid cells are independent across the original group boundaries. The statistical presence of agglomeration shadows is also not sensitive to increasing the group size to 1/4-degree by 1/4-degree (Appendix Figure A.19), approximately 25km by 25km. It is computationally intensive to allow for a smooth decay in spatial correlation across the 2.3 million grid cells, following Conley (1999), but the statistical inference is similar with a linear decay in spatial correlation around each grid cell up to a distance cutoff of 4km (Appendix Figure A.20) or 8km (Appendix Figure A.21).

IV.C   Competition Across Cities versus Across Ports

Cities seeded at ancient ports appear to cast agglomeration shadows that discourage nearby city formation, consistent with simulations in Section I. One potential mechanism is that ports themselves make nearby ports less needed and thereby discourage city formation at nearby ports. We find little evidence for this port competition, however, and more evidence

for city competition, in which cities discourage nearby city formation largely separate from impacts through port structures themselves.

To explore these mechanisms, we restrict our sample to grid cells with ancient ports and estimate how the loss of natural harbors influences that grid cell and surrounding grid cells:

$$(3) \qquad Y_i = \beta_1 NoHarbor_i + \beta_2 SurroundingShareNoHarbor_i + \theta \mathbf{X}_i + \varepsilon_i.$$

Outcomes Y_i include whether that grid cell has modern port structures, along with log population density and indicators for log population density exceeding 6 (urban activity) or 9 (city activity). The coefficient β_1 reports differences for ancient port grid cells that have since lost their natural harbor, compared to ancient port grid cells that still have a natural harbor. The coefficient β_2 reports differences when a greater share of ancient port grid cells within 5-50km have lost their natural harbor. We control for the number of other ancient port grid cells within 5-50km, in $\mathbf{X_i}$, along with our other baseline controls (log distance to the coast; log distance to the nearest major river; latitude; longitude; terrain ruggedness; and average temperature and precipitation in both January and July).[15]

Table 3 reports that losing a natural harbor substantially decreases the probability of that grid cell having a modern port structure (Column 1, row 1). However, when surrounding ancient ports have lost their natural harbor, and are thereby less likely to have modern port structures, there is no increase in the likelihood of that grid cell having port structures (Column 1, row 2). This suggests that nearby ports do not systematically crowd-out (or crowd-in) port activity through direct competition (or collaboration).

Table 3 also reports that losing a natural harbor decreases that grid cell's average population density, likelihood of urban activity, and likelihood of city activity (Columns 2-4, row 1). These outcomes are greater, however, when surrounding ancient ports have lost their natural harbor and thereby have lower population density (Columns 2-4, row 2).[16] This suggests that cities themselves are in competition, with increased economic activity in a grid cell from decreased surrounding economic activity.

V Modern City Spacing: Realized versus Random

This section considers the general spacing between all modern cities in our sample region, which complements our earlier analysis of agglomeration shadows around ancient port locations. Our previous analysis explores how the evolved spatial structure responds to particular stimuli over a long time horizon, from the need for many shelter points along the coast in the

---

[15]For this specification, we omit 71 ancient port grid cells that have no other ancient port within 5-50km.

[16]By contrast, if spatially correlated historical shocks induce local harbor loss and lower local economic activity, this would generate a negative relationship between grid cell economic activity and surrounding harbor loss.

ancient era, whereas this last exercise characterizes spatial patterns in that evolved urban hierarchy. In such analyses of the modern cross-section, city locations are taken as given and their spacing is characterized, once their size and location have co-evolved with their surroundings.

We now consider the distance between each city and its nearest city, and explore whether the realized distribution of minimum distances is distinct from a simulated random distribution. Agglomeration shadows would result in fewer-than-expected cities with close neighbors, with more-than-expected nearest neighbors after emerging from that shadow. In focusing on the distribution of minimum city distances, with a distribution-free test based on a simulated random null, this exercise differs from other work in economic geography that characterizes the equilibrium spatial distribution of cities (Dobkins and Ioannides, 2001; Ioannides and Overman, 2004; Rauch, 2014; Mori, Smith, and Hsu, 2020; Henderson, Peng, and Venables, 2022; Mori et al., 2023). Our analysis is related to a "dartboard" approach to measuring industry-level agglomeration (Ellison and Glaeser, 1997, 1999; Duranton and Overman, 2005), which compares observed patterns to what could be expected by random chance.

Our analysis here is similar to an approach in biology to characterize the spatial distribution of tree seedlings (Diggle, 1983). We adjust this approach for an economic geography context, however. Rather than drawing purely random city locations, we predict city likelihood based on grid cell characteristics and use the fitted value for each grid cell as a probability weight when drawing different random locations for cities.[17] For example, this allows for the random locations of cities to be systematically close to the coast. More suitable geographic locations for cities are positively spatially correlated, with respect to the observed characteristics. If the remaining unobserved characteristics are also (conditionally) positively spatially correlated, the random benchmark will be too spaced apart, making it difficult to detect agglomeration shadows.

We use GHSL data for urban center locations in our sample region, and implement our analysis separately for cities in three population size categories: over 500k, over 250k, and over 100k. This exercise relies on administrative city boundaries from GHSL, rather than grid cell data, because two nearby dense grid cells could be part of the same city. Further, population density varies across different cutoffs within a city. However, greater population density is correlated with greater city population.[18]

Figure 8, Panel A, shows that modern large cities are less likely to have neighbors within

---

[17]For this prediction, we use a probit model with country fixed effects and the baseline geography controls from equations (1) and (2). This ensures positive weights, which are less than one, and restricts city locations to countries with cities in our sample region.

[18]The correlation between log population and log population density is 0.37. Cities with greater population are also more likely to have grid cells with log population density above 9.

40km, and more likely to have neighbors within 40-60km, consistent with agglomeration shadows around large cities and the relative success of cities just beyond those shadows. The red line shows the realized cumulative density function (CDF) of minimum distances between the 61 modern large cities and their nearest large city. The black lines show the CDF from a weighted random draw of 61 city locations in 1,000 simulations, graphing the median along with the 5th centile and 95th centile. For the red line to be to the right of the thin black line, it means that the realized distribution of modern cities has fewer nearest neighbors within that distance than 95% of randomly drawn city locations. When the red line increases faster than the black lines, there are more observed nearest neighbors at that distance than would be expected by random chance.

Panels C and E of Figure 8 show that agglomeration shadows are less pronounced when including smaller cities. The observed CDF is somewhat distinct from random simulations at some initial distances, before increasing more rapidly, but this difference is less substantial than for the largest cities.

Using defined "city" locations to measure agglomeration shadows raises a potential measurement concern: the area just outside a defined city may not be another city because, if it were, it may have been included in that first defined city.[19] We can adjust for this effect by shifting the simulated distribution of cities, however, using the variation in city sizes to construct non-overlapping circles around cities: if we randomly draw another city within that circle, we drop it and draw another city.[20] This shifts the simulated distributions to the right, as shown in Panels B, D, and F of Figure 8. There are still fewer-than-expected large cities within 40km of other large cities and more catch-up between 40-60km (Panel B), but there are no longer detectable agglomeration shadows for cities with population above 250k or 100k (Panels D and F).

These results are consistent with agglomeration shadows around large cities, despite the potential for spatially-correlated location fundamentals and particular shocks accumulated over the course of millennia that might lead to more close-by cities than we would expect by chance.

---

[19]That is, cities may indeed develop near each other but become considered one large city: when the locations of city boundaries and city centers are defined ex post, along with the concurrent development of surrounding areas, these definitions could overstate agglomeration shadows. For example, if the boundary of a large city is drawn such that it contains nearby densely populated areas, then areas just outside that boundary will mechanically have low population density.

[20]For each city, we take the square root of its area over π to define the radius of a circle that approximates that city's geographic footprint. When redrawing cities, we randomly assign each real radius to each drawn city. Drawing is done sequentially, such that we draw a city randomly, then randomly assign a radius, and then redraw if, for any other already-drawn city, the distance between the new city and the already-drawn city is less than the sum of their radii. Otherwise, this drawn city is kept and its radius cannot be assigned again.

VI   Conclusion

The location of economic activity has direct implications for landowners and, since people are generally not perfectly mobile, also for individuals' well-being more generally. Indeed, a motivation for place-based policies is to assist people in targeted locations by encouraging local growth. Locally successful policy may discourage similar growth nearby, however, in models in which concentrations of economic activity compete with and discourage rival centers caught in their "agglomeration shadow."

We focus on identifying agglomeration shadows, using ancient ports as seeds from which cities emerged. The locations of ancient ports, which were shaped by very local coastline features, provide empirical traction to explore impacts on nearby places. Ancient port locations may themselves continue to benefit from their local geography, but these locations are plausibly uncorrelated with a down-and-up wave in unobservable grid cell characteristics 20km and 40km away. Further, where natural harbors survived in these ancient port locations, the location of modern cities was more precisely pinned down, mitigating the problem of wave interference. Where harbors did not survive, even with strong agglomeration shadows, the alternating peaks and valleys in economic activity can average out and appear as smooth declines in economic activity.

We estimate agglomeration shadows in city formation, which appear as a distinctive down-and-up wave in city formation. Large cities are less likely to form at intermediate distances from ancient ports, caught in the agglomeration shadow of cities seeded at ancient port locations. Cities are more likely to form at further distances, however, just beyond that shadow. This contrasts with a more general decline in population density and urban activity in distance to the ancient port, which is consistent with nearby places becoming confined to second-tier status within an urban hierarchy. Nearby harbor loss also does not directly affect own port activity in the modern era, positively or negatively, but does influence the urban hierarchy.

Setting aside the ancient port locations, we show that the spacing between all large cities is statistically distinct from random. There are fewer large cities at intermediate distances than we would expect at random, after accounting for locational fundamentals. In characterizing the cross-sectional spatial distribution of economic activity, this analysis complements our study of the emergence of city spacing in response to particular stimuli from ancient port locations.

Early investments in local economic activity can generate sustained long-run local growth, and we extend this literature to identify further impacts on the spatial organization of economic activity in the surrounding urban hierarchy. When economic activity clusters in a location, an "agglomeration shadow" can discourage some economic activities in nearby

locations until sufficient distance makes rival centers viable.

References

Abulafia, David. 2011. *The Great Sea: A Human History of the Mediterranean.* London: Allen Lane.

Accetturo, Antonio, Michele Cascarano, and Guido de Blasio. 2019. "Pirate Attacks and the Shape of the Italian Urban System." Working Paper.

Ahlfeldt, Gabriel M., and Nicolai Wendland. 2013. "How Polycentric is a Monocentric City? Centers, Spillovers and Hysteresis." *Journal of Economic Geography*, 13(1): 53–83.

Ahlfeldt, Gabriel M., Stephen J. Redding, Daniel M. Sturm, and Nikolaus Wolf. 2015. "The Economics of Density: Evidence from the Berlin Wall." *Econometrica*, 83(6): 2127–2189.

Ahmad, Zofia, and Luke Chicoine. 2021. "Silk Roads to Riches: Persistence Along an Ancient Trade Network." Working Paper.

Ali, Kamar, M. Rose Olfert, Mark D. Partridge, and Dan S. Rickman. 2009. "Do New Economic Geography Agglomeration Shadows Underlie Current Population Dynamics across the Urban Hierarchy?" *Papers in Regional Science*, 88(2): 445–467.

Alonso, William. 1964. *Location and Land Use: Toward a General Theory of Land Rent.* Cambridge, MA: Harvard University Press.

Bakker, Jan David, Stephan Maurer, Jörn-Steffen Pischke, and Ferdinand Rauch. 2021. "Of Mice and Merchants: Connectedness and the Location of Economic Activity in the Iron Age." *Review of Economics and Statistics*, 103(4): 652–665.

Barjamovic, Gojko, Thomas Chaney, Kerem Coşar, and Ali Hortaçsu. 2019. "Trade, Merchants, and the Lost Cities of the Bronze Age." *Quarterly Journal of Economics*, 134(3): 1455–1503.

Barsanetti, Bruno. 2023. "Road Endpoints and City Sizes." *Review of Economics and Statistics*, 1–45.

Beltrán Tapia, Francisco J., Alfonso Díez-Minguela, and Julio Martinez-Galarraga. 2021. "The Shadow of Cities: Size, Location and the Spatial Distribution of Population." *Annals of Regional Science*, 66: 729–753.

Bleakley, Hoyt, and Jeffrey Lin. 2012. "Portage and Path Dependence." *Quarterly Journal of Economics*, 127(2): 587–644.

Bloom, Nicholas, Erik Brynjolfsson, Lucia Foster, Ron Jarmin, Megha Patnaik, Itay Saporta-Eksten, and John Van Reenen. 2019. "What Drives Differences in Management Practices?" *American Economic Review*, 109(5): 1648–1683.

Bosker, Maarten, and Eltjo Buringh. 2017. "City Seeds: Geography and the Origins of the European City System." *Journal of Urban Economics*, 98: 139–157.

Brooks, Leah, Nicolas Gendron-Carrier, and Gisela Rua. 2021. "The Local Impact of Containerization." *Journal of Urban Economics*, 126.

Center for International Earth Science Information Network (CIESIN). 2011. "Global Rural-Urban Mapping Project (GRUMPv1): Population Density Grid." Palisades, NY: NASA Socioeconomic Data and Applications Center. Version 1. Accessed 2021.

Center for International Earth Science Information Network (CIESIN). 2018. "Gridded Population of the World (GPWv4): Population Density." Palisades, NY: NASA Socioeconomic Data and Applications Center. Version 4, Revision 11. Accessed 2021.

Christaller, Walter. 1933. *Die Zentralen Orte in Süddeutschland.* Translated in 1966 by C.W. Baskin to The Central Places in Southern Germany. Englewood Cliffs, NJ: Prentice-Hall.

Conley, Timothy G. 1999. "GMM Estimation with Cross Sectional Dependence." *Journal of Econometrics*, 92(1): 1–45.

Costinot, Arnaud, Dave Donaldson, Margaret Kyle, and Heidi Williams. 2019. "The More We Die, the More We Sell? A Simple Test of the Home-Market Effect." *Quarterly Journal of Economics*, 134(2): 843–894.

Cuberes, David, Klaus Desmet, and Jordan Rappaport. 2021. "Urban Growth Shadows." *Journal of Urban Economics*, 123: 103334.

Cummins, Steven, and Sally Macintyre. 2002. "'Food Deserts' — Evidence and Assumption in Health Policy Making." *BMJ*, 325(7361): 436–438.

Dalgaard, Carl-Johan, Anne Sofie B. Knudsen, and Pablo Selaya. 2020. "The Bounty of the Sea and Long-Run Development." *Journal of Economic Growth*, 25(3): 259–295.

Dalgaard, Carl-Johan, Nicolai Kaarsen, Ola Olsson, and Pablo Selaya. 2022. "Roman Roads to Prosperity: Persistence and Non-Persistence of Public Infrastructure." *Journal of Comparative Economics*, 50(4): 896–916.

Davis, Donald R., and Jonathan I. Dingel. 2020. "The Comparative Advantage of Cities." *Journal of International Economics*, 123: 103291.

de Benedictis, Luca, Vania Licio, and Anna Maria Pinna. 2023. "From the Historical Roman Road Network to Modern Infrastructure in Italy." *Journal of Regional Science*, 63(5): 1162–1191.

de Graauw, Arthur. 2019. "The Catalogue of Ancient Coastal Settlements, Ports and Harbours." Accessed 2019. https://www.ancientportsantiques.com/.

Diggle, Peter J. 1983. *Statistical Anaylsis of Spatial Point Patterns.* London: Academic Press.

Dingel, Jonathan I., Joshua D. Gottlieb, Maya Lozinski, and Pauline Mourot. 2023. "Market Size and Trade in Medical Services." Working Paper.

Dobkins, Linda Harris, and Yannis M. Ioannides. 2001. "Spatial Interactions Among US Cities: 1900–1990." *Regional science and Urban Economics*, 31(6): 701–731.

Donaldson, Dave, and Richard Hornbeck. 2016. "Railroads and American Economic Growth: A "Market Access" Approach." *Quarterly Journal of Economics*, 131(2): 799–858.

Ducruet, César, Réka Juhász, Dávid Krisztián Nagy, and Claudia Steinwender. 2024. "All Aboard: The Effects of Port Development." Conditionally Accepted.

Duranton, Gilles, and Diego Puga. 2004. "Micro-Foundations of Urban Agglomeration Economies." In *Handbook of Regional and Urban Economics*. Vol. 4, 2063–2117. Amsterdam: Elsevier.

Duranton, Gilles, and Henry G. Overman. 2005. "Testing for Localization Using Micro-Geographic Data." *Review of Economic Studies*, 72(4): 1077–1106.

Ellison, Glenn, and Edward L. Glaeser. 1997. "Geographic Concentration in US Manufacturing Industries: A Dartboard Approach." *Journal of Political Economy*, 105(5): 889–927.

Ellison, Glenn, and Edward L. Glaeser. 1999. "The Geographic Concentration of Industry: Does Natural Advantage Explain Agglomeration?" *American Economic Review*, 89(2): 311–316.

Ellison, Glenn, Edward L. Glaeser, and William R. Kerr. 2010. "What Causes Industry Agglomeration? Evidence from Coagglomeration Patterns." *American Economic Review*, 100(3): 1195–1213.

Faber, Benjamin. 2014. "Trade Integration, Market Size, and Industrialization: Evidence from China's National Trunk Highway System." *Review of Economic Studies*, 81(3 (288)): 1046–1070.

Finkelstein, Amy, Matthew Gentzkow, and Heidi Williams. 2021. "Place-Based Drivers of Mortality: Evidence from Migration." *American Economic Review*, 111(8): 2697–2735.

Florczyk, A., C. Corbane, M. Schiavina, M. Pesaresi, L. Maffenini, M. Melchiorri, P. Politis, F. Sabo, S. Freire, D. Ehrlich, T. Kemper, P. Tommasi, D. Airaghi, and L. Zanchetta. 2019. "GHS-UCDB R2019A: GHS Urban Centre Database 2015, Multitemporal and Multidimensional Attributes." Brussels: European Commission, Joint Research Centre (JRC), Global Human Settlement Layer (GHSL). Accessed 2021.

Flückiger, Matthias, Erik Hornung, Mario Larch, Markus Ludwig, and Allard Mees. 2021. "Roman Transport Network Connectivity and Economic Integration." *Review of Economic Studies*, 89(2): 774–810.

Franco, Ana Paula, Sebastian Galiani, and Pablo Lavado. 2021. "Long-Term Effects of the Inca Road." Working Paper.

Fujita, Masahisa, and Paul R. Krugman. 1995. "When is the Economy Monocentric?: Von Thünen and Chamberlin Unified." *Regional Science and Urban Economics*, 25(4): 505–528.

Fujita, Masahisa, and Tomoya Mori. 1996. "The Role of Ports in the Making of Major Cities: Self-Agglomeration and Hub-Effect." *Journal of Development Economics*, 49(1): 93–120.

Fujita, Masahisa, and Tomoya Mori. 2005. "Frontiers of the New Economic Geography." *Papers in Regional Science*, 84(3): 377–405.

Fujita, Masahisa, Paul R. Krugman, and Anthony Venables. 1999. *The Spatial Economy: Cities, Regions, and International Trade.* Cambridge, MA: MIT press.

Fujita, Masahisa, Paul R. Krugman, and Tomoya Mori. 1999. "On the Evolution of Hierarchical Urban Systems." *European Economic Review*, 43(2): 209–251.

Gabaix, Xavier. 1999. "Zipf's Law for Cities: An Explanation." *Quarterly Journal of Economics*, 114(3): 739–767.

Giroud, Xavier, Simone Lenzu, Quinn Maingi, and Holger Mueller. 2021. "Propagation and Amplification of Local Productivity Spillovers." Working Paper.

Glaeser, Edward L., and Joshua D. Gottlieb. 2009. "The Wealth of Cities: Agglomeration Economics and Spatial Equilibrium in the United States." *Journal of Economic Literature*, 47(December): 983–1028.

Greenstone, Michael, Richard Hornbeck, and Enrico Moretti. 2010. "Identifying Agglomeration Spillovers: Evidence from Winners and Losers of Large Plant Openings." *Journal of Political Economy*, 118(3): 536–598.

Greif, Avner. 1993. "Contract Enforceability and Economic Institutions in Early Trade: The Maghribi Traders' Coalition." *American Economic Review*, 525–548.

Hall, Jacob. 2023. "Travel Speed over the Longue Durée." Working Paper.

Hanson, J.W. 2016. "Cities Database." Oxford: Oxford Roman Economy Project (OXREP). Version 1.0. Accessed July 2020. http://www.romaneconomy.ox.ac.uk/.

Helpman, Elhanan, and Paul Krugman. 1985. *Market Structure and Foreign Trade.* Cambridge, MA: MIT Press.

Henderson, J. Vernon. 1974. "The Sizes and Types of Cities." *American Economic Review*, 64(4): 640–656.

Henderson, J. Vernon, Cong Peng, and Anthony Venables. 2022. "Growth in the African Urban Hierarchy." Working Paper.

Hornbeck, Richard, and Martin Rotemberg. 2024. "Growth Off the Rails: Aggregate Productivity Growth in Distorted Economies." *Journal of Political Economy*, Forthcoming.

International Institute for Applied Systems Analysis (IIASA) and Food and Agriculture Organization of the United Nations (FAO). 2020. "Global Agro-Ecological Zones (GAEZ)." Laxenburg, Austria: IIASA; Rome: FAO. Version 4.0. Accessed June 2024.

Ioannides, Yannis M., and Henry G. Overman. 2004. "Spatial Evolution of the US Urban System." *Journal of Economic Geography*, 4(2): 131–156.

Jefferson, Mark. 1939. "The Law of the Primate City." *Geographical Review*, 29(2): 226–232.

Kaschner, K., K. Kesner-Reyes, C. Garilao, J. Segschneider, T. Rius-Barile, J. Rees, and R. Froese. 2019. "AquaMaps: Predicted Range Maps for Aquatic Species." Accessed May 2024.

Lösch, August. 1940. *Die Räumliche Ordnung der Wirtschaft.* Translated in 1954 by Jena Fischer to The Economics of Location. New Haven, CT: Yale University Press.

Marshall, Alfred. 1890. *Principles of Economics.* London: Macmillan and Co.

Matsuyama, Kiminori. 2017. "Geographical Advantage: Home Market Effect in a Multi-Region World." *Research in Economics*, 71(4): 740–758.

Maurer, Stephan, and Ferdinand Rauch. 2022. "Economic Geography Aspects of the Panama Canal." *Oxford Economic Papers*, 75(1): 142–162.

Michaels, Guy, and Ferdinand Rauch. 2018. "Resetting the Urban Network: 117–2012." *Economic Journal*, 128(608): 378–412.

Mills, Edwin S. 1967. "An Aggregative Model of Resource Allocation in a Metropolitan Area." *American Economic Review*, 57(2): 197–210.

Mori, Tomoya, and Tony E Smith. 2015. "On the Spatial Scale of Industrial Agglomerations." *Journal of Urban Economics*, 89: 1–20.

Mori, Tomoya, Takashi Akamatsu, Yuki Takayama, and Minoru Osawa. 2023. "Origin of Power Laws and Their Spatial Fractal Structure for City-Size Distributions." Working Paper.

Mori, Tomoya, Tony E. Smith, and Wen-Tai Hsu. 2020. "Common Power Laws for Cities and Spatial Fractal Structures." *Proceedings of the National Academy of Sciences*, 117(12): 6469–6475.

Muth, Richard. 1969. *Cities and Housing : The Spatial Pattern of Urban Residential Land Use.* Chicago: University of Chicago Press.

Nunn, Nathan, and Diego Puga. 2012. "Ruggedness: The Blessing of Bad Geography in Africa." *Review of Economics and Statistics*, 94(1): 20–36. Accessed replication data September 2019. https://diegopuga.org/data/rugged/.

Nunn, Nathan, and Nancy Qian. 2011. "The Potato's Contribution to Population and Urbanization: Evidence From A Historical Experiment." *Quarterly Journal of Economics*, 126(2): 593–650.

Rauch, Ferdinand. 2014. "Cities as Spatial Clusters." *Journal of Economic Geography*, 14(4): 759–773.

Redding, Stephen J, and Daniel M. Sturm. 2008. "The Costs of Remoteness: Evidence from German Division and Reunification." *American Economic Review*, 98(5): 1766–1797.

Scheidel, Walter. 2015. "Orbis: The Stanford Geospatial Network Model of the Roman World." Working Paper.

Schiavina, Marcello, Sergio Freire, and Kytt MacManus. 2019. "GHS-POP R2019A - GHS Population Grid Multitemporal (1975-2015)." Brussels: European Commission, Joint Research Centre (JRC), Global Human Settlement Layer (GHSL). Accessed 2021.

Talbert, Richard L.A., ed. 2000. *Barrington Atlas of the Greek and Roman World.* Princeton, NJ: Princeton University Press.

Tervo, Hannu. 2010. "Cities, Hinterlands and Agglomeration Shadows: Spatial Developments in Finland During 1880–2004." *Explorations in Economic History*, 47(4): 476–486.

von Thünen, Johann Heinrich. 1826. *Der Isolierte Staat.* Edited by Peter Hall. Translated in 1966 by Carla M. Wartenberg to Von Thünen's Isolated State: An English Edition of Der Isolierte Staat. Oxford: Pergamon Press.

Figure 1. Share of Instances with Cities by Distance to Fixed Starting City

Panel A. Any City (≥1 Industry)   Panel B. Large City (≥2 Industries)
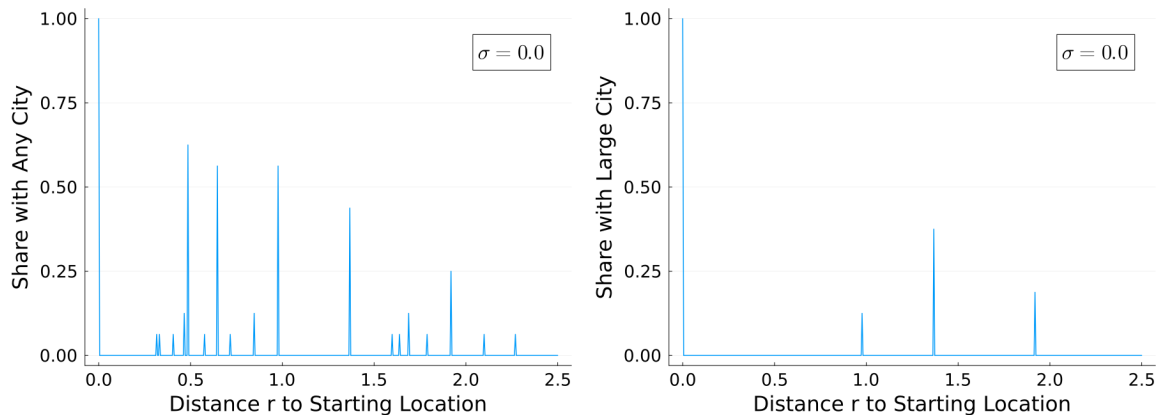
Notes: This figure shows the share of instances in which there is a city at the indicated distance r from a fixed starting city, as modeled for the 16 aggregate population parameter values in Figure 7 of Fujita, Krugman, and Mori (1999). Four of these 16 values are bifurcation values, where cities are "born" or "die" or change their number of industries, and we use city locations on the right side of the bifurcation associated with larger population.

    Panel A shows the share of instances with any city at that distance r, defined as a location with at least one manufacturing industry. Panel B shows the share of instances with a large city at that distance r, defined as a location with at least 2 manufacturing industries. The distance r is restricted to the positive direction, along this one-dimensional economy, from the location of the fixed initial city at distance 0.

Figure 2. Share of Simulations with Cities by Distance to Fixed Starting Location, with Increasing Spatial Noise

Panel A. Any City, with Low Noise
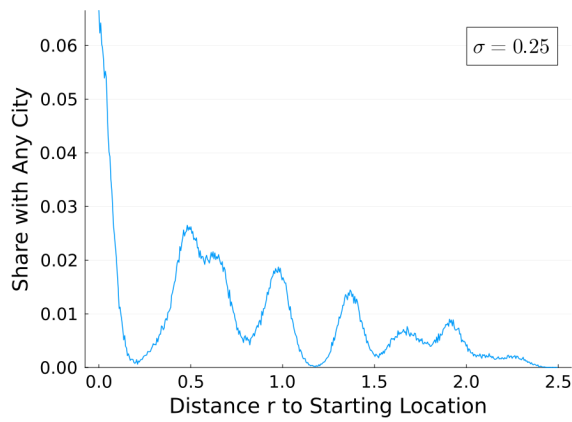
Panel B. Large City, with Low Noise
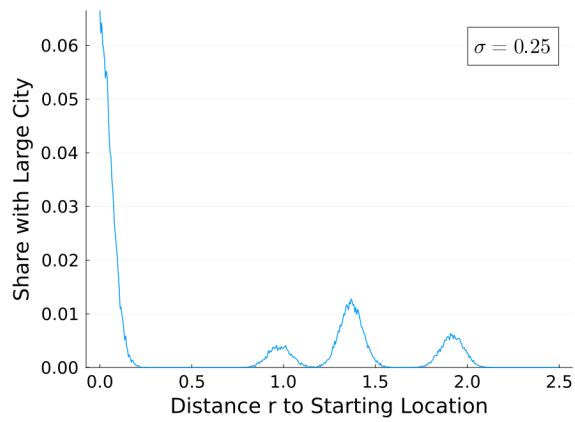
Panel C. Any City, with Medium Noise
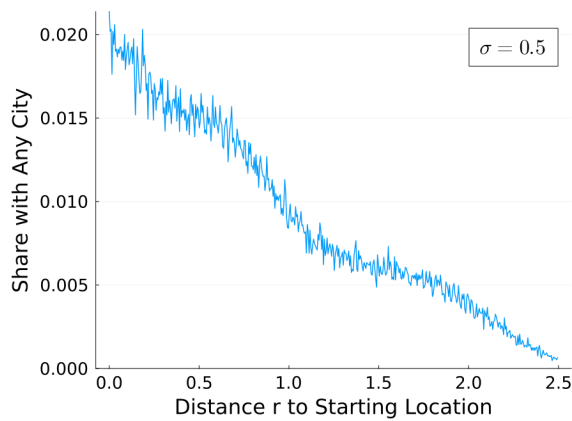
Panel D. Large City, with Medium Noise
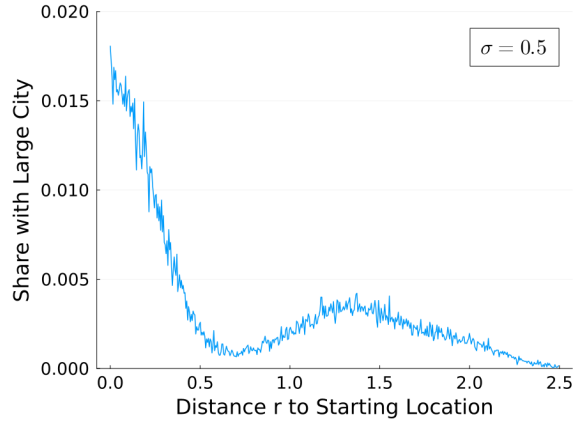
Panel E. Any City, with High Noise
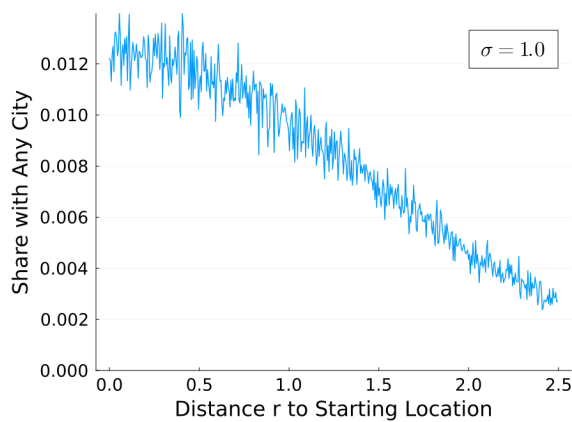
Panel F. Large City, with High Noise
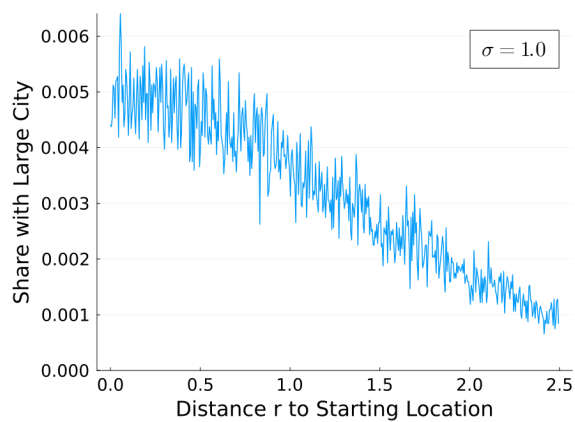
Notes: Each panel reports the share of simulations in which there is a city at the indicated distance r from a fixed starting location. In each of 2,000 simulations, we shift the city locations from Figure 1 left or right by a spatial noise term drawn from a mean zero normal distribution with increasing standard deviation: "Low Noise" ($\sigma = 0.25$) in Panels A and B; "Medium Noise" ($\sigma = 0.5$) in Panels C and D; and "High Noise" ($\sigma = 1.0$) in Panels E and F. The distance r is restricted to the positive direction from the location of the fixed starting location at distance 0 (which can now differ from the location of that previously central initial city).

Figure 3. Share of Simulations with Cities by Distance: Medium versus High Noise

Panel A. Any City, Medium and High Noise
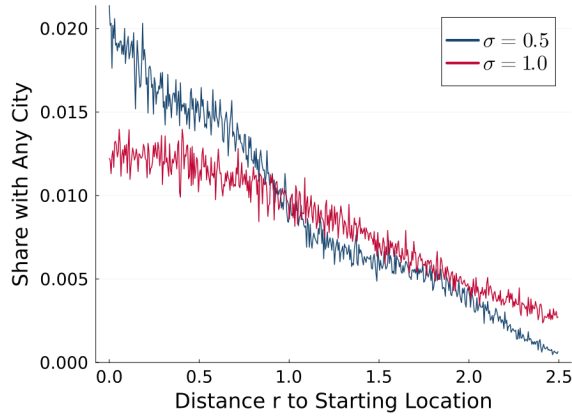
Panel B. Large City, Medium and High Noise
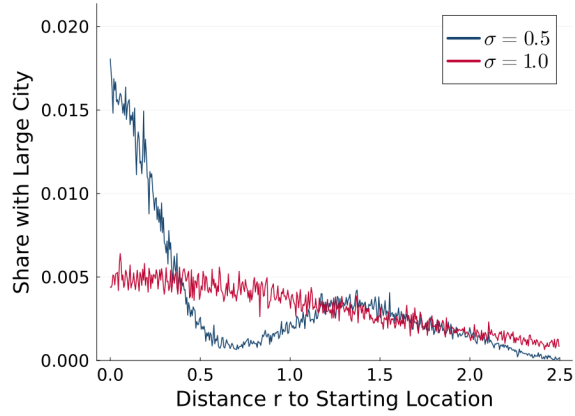
Panel C. Any City, Difference between Medium and High Noise
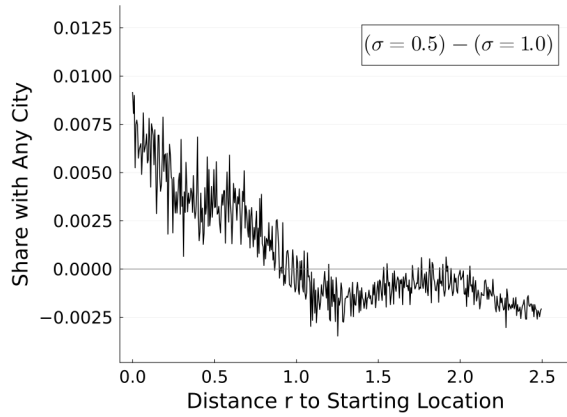
Panel D. Large City, Difference between Medium and High Noise
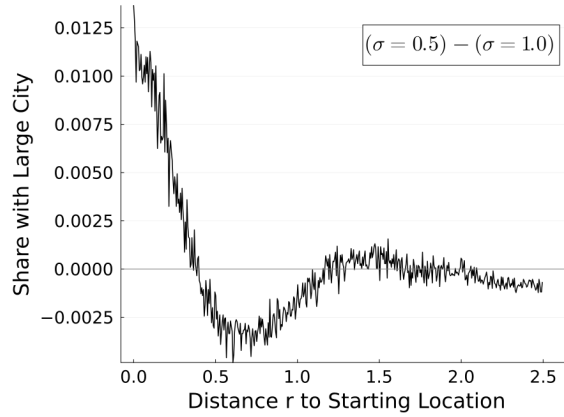
Notes: This figure compares the "Medium Noise" and "High Noise" cases from Figure 2. Panels A and B show simulations with Medium and High Noise on the same plot, and Panels C and D show the difference in shares (Medium Noise minus High Noise).

Figure 4. Ancient Port Locations in Our Main Sample

Panel A. All Ancient Ports
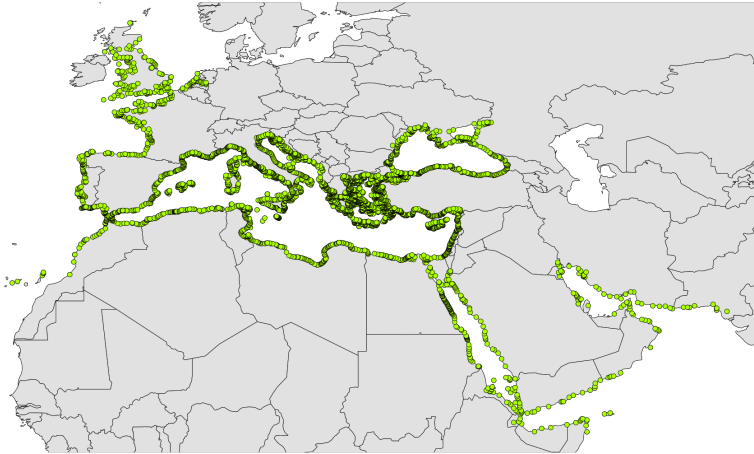
Panel B. Ancient Ports with a Modern Natural Harbor

Panel C. Ancient Ports without a Modern Natural Harbor
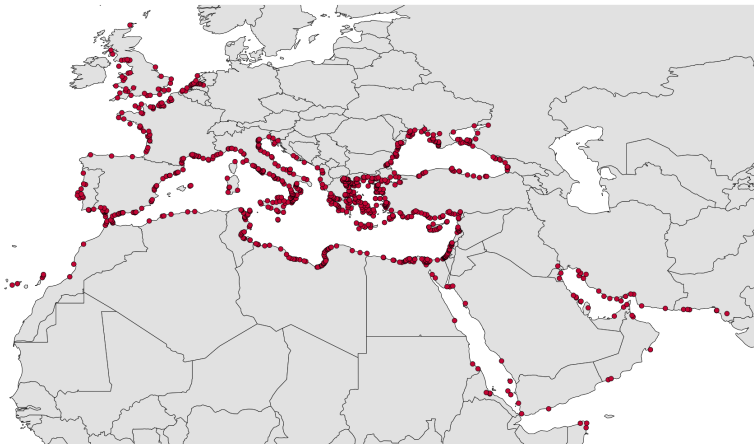
Notes: This figure shows the locations of ancient ports in our main sample. Panel A shows all ancient ports, Panel B shows ancient port locations that have a natural harbor in modern satellite images, and Panel C shows ancient port locations that do not have a natural harbor in modern satellite images.

Figure 5. Impacts on Average Log Population Density,
by Distance to Nearest Ancient Port
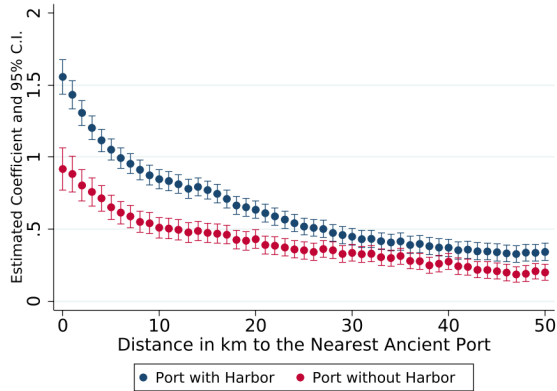
Notes: This figure shows impacts on average log density by distance to the nearest ancient port with and without a natural harbor, from estimating equation (2). The sample is 1km-by-1km grid cells within 50km of the coast, and include the baseline controls: log distance to the coast, log distance to the nearest major river, latitude, longitude, terrain ruggedness, and average temperature and precipitation in both January and July.

Vertical lines report 95% confidence intervals, based on robust standard errors clustered at 1/12-degree-by-1/12-degree groups (roughly 8km-by-8km in the middle of our sample region).

Figure 6. Impacts on Probability of Urban Density or City Density, by Distance to Nearest Ancient Port

Panel A. Probability of Urban Density
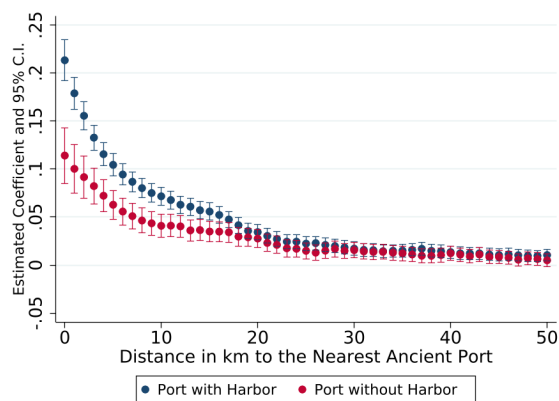
Panel B. Probability of City Density
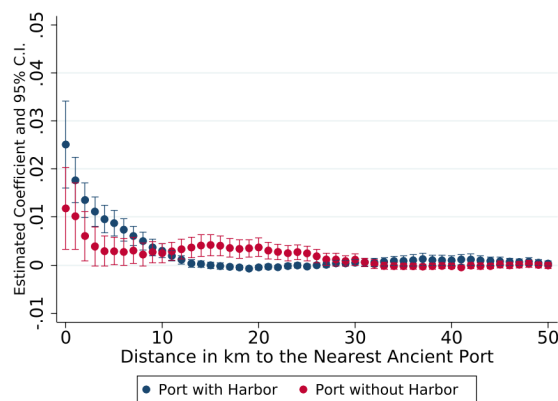
Panel C. Differences for Urban Density
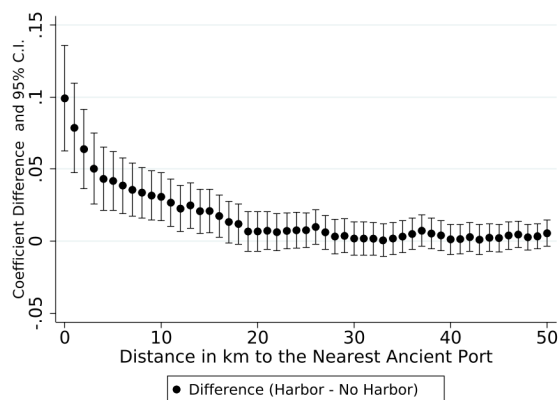
Panel D. Differences for City Density
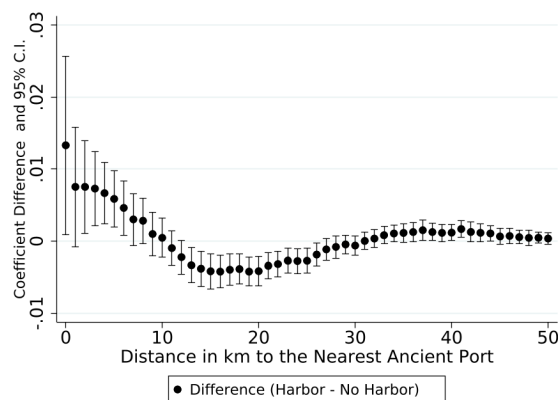
Notes: This figure shows impacts on the probability of a grid cell having "Urban Density" (ln population density > 6) or "City Density" (ln population density > 9), by distance to the nearest ancient port with and without a natural harbor, from estimating equation (2). The sample is 1km-by-1km grid cells within 50km of the coast, and include the baseline controls: log distance to the coast, log distance to the nearest major river, latitude, longitude, terrain ruggedness, and average temperature and precipitation in both January and July.

Panels A and B show coefficients on distance to the nearest ancient port with a modern natural harbor (blue circle) and without a modern natural harbor (red circle). Panels C and D show the differences between these estimates (with harbor minus without harbor).

Vertical lines report 95% confidence intervals, based on robust standard errors clustered at 1/12-degree-by-1/12-degree groups (roughly 8km-by-8km in the middle of our sample region).

Figure 7. Impacts on Probability of Urban Density or City Density, with Fitted Log Relationship

Panel A. Probability of Urban Density
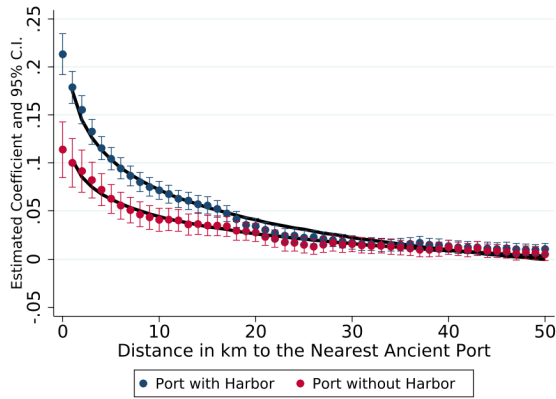
Panel B. Probability of City Density
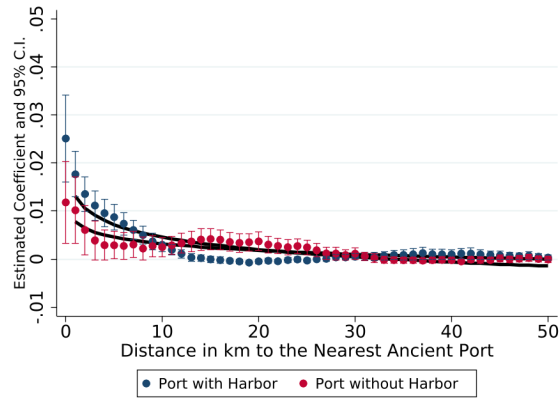
Panel C. Urban, Difference from Log Fit
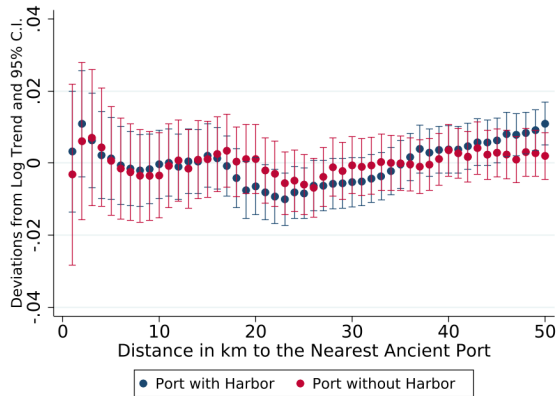
Panel D. City, Difference from Log Fit
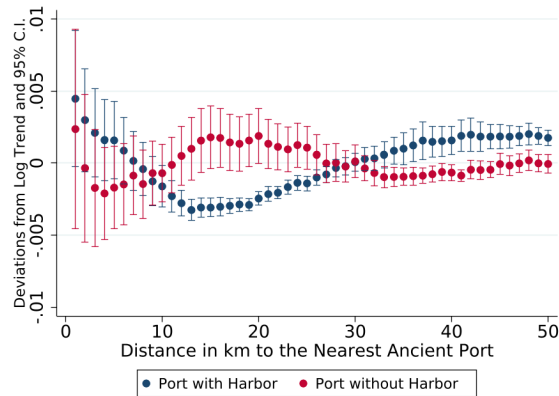
Notes: Panels A and B reproduce Panels A and B from Figure 6, with the addition of two black lines that represent the fitted log relationships from regressing the coefficients from distance bins 1–50 on log distance. Panels C and D report the coefficients from Panels A and B, subtracting the fitted log relationships (black lines). Vertical lines report 95% confidence intervals using the standard errors from Panels A and B.

34

Figure 8. Modern City Spacing: Realized versus Random

Panel A. Cities with Population above 500k
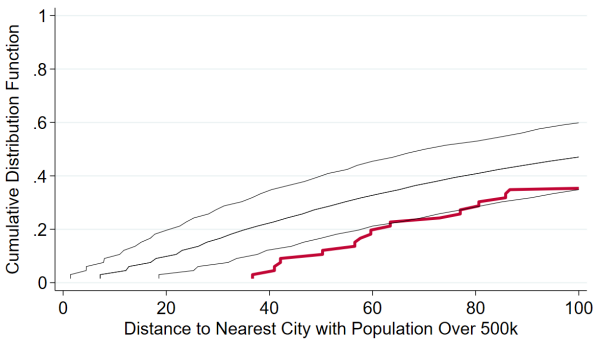
Panel B. Cities with Population above 500k, with Area Adjustment
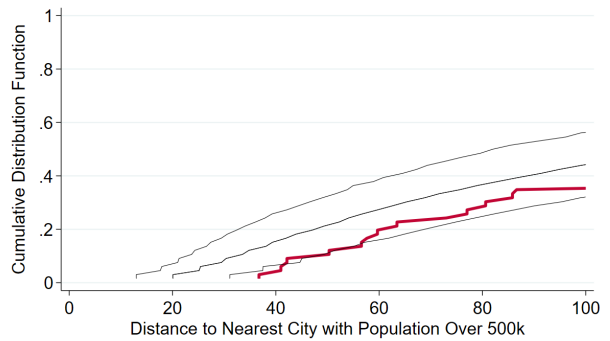
Panel C. Cities with Population above 250k
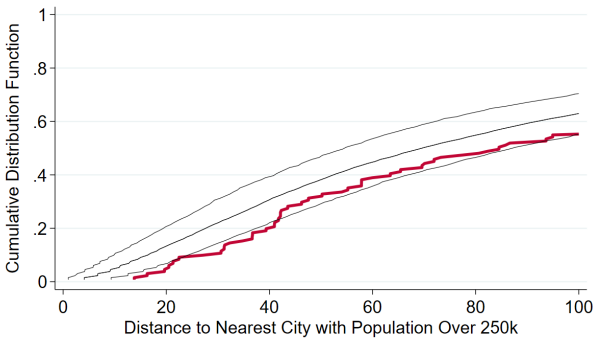
Panel D. Cities with Population above 250k, with Area Adjustment
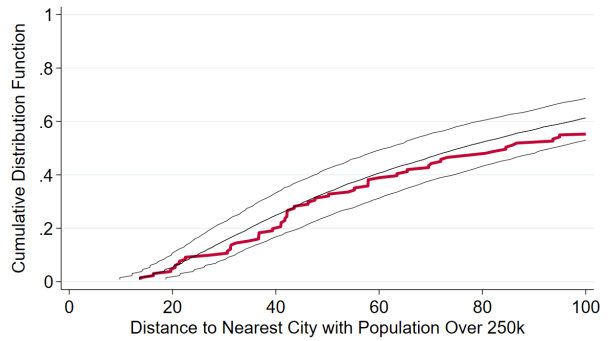
Panel E. Cities with Population above 100k
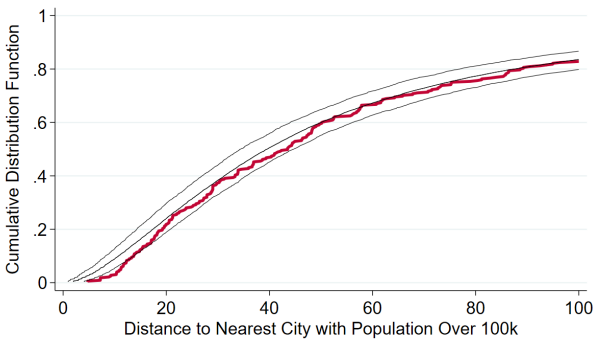
Panel F. Cities with Population above 100k, with Area Adjustment
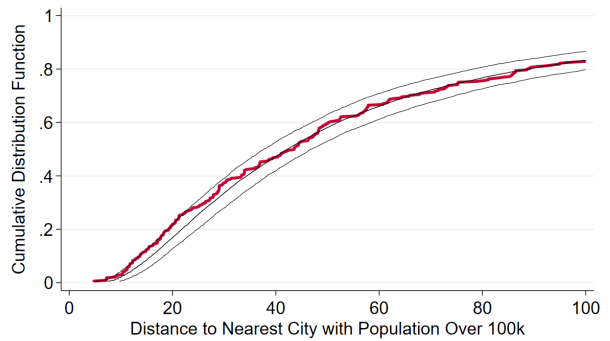
Notes: This figure compares real and simulated distributions of distances between nearest cities, by city size. The red line shows the real distribution of distances to cities. The central gray line shows the median simulated distance, and the upper and lower gray lines show the 5th and 95th percentiles. We identify real city locations and their 2015 populations using GHSL data. The distributions of random city locations are randomly drawn 1,000 times from our baseline grid sample. For each city size category, the random draws use probability weights for each grid cell based on its fitted value from a probit model predicting city likelihood with country fixed effects and the baseline controls: log distance to the coast, log distance to the nearest major river, latitude, longitude, terrain ruggedness, and average temperature and precipitation in both January and July. For Panels B, D, and F, the "Area Adjustment" to the simulated black lines refers to when cities are redrawn if they are within the geographic footprint of an already-placed city, as described in Section V. The figure is truncated at 100km.

Table 1. Estimated Impacts of Ancient Ports on Grid Cell Population Density

	Ln Population Density (1)	Urban Density (2)	City Density (3)
Panel A.			
Ancient Port	0.589	0.116	0.017
	(0.044)	(0.008)	(0.004)
Panel B.			
Barrington 1 City	3.867	0.663	0.395
	(0.675)	(0.124)	(0.155)
Barrington 2 City	2.423	0.418	0.114
	(0.217)	(0.048)	(0.032)
Barrington 3 City	1.714	0.308	0.038
	(0.098)	(0.022)	(0.009)
Outcome Mean	3.290	0.071	0.002
	[1.888]	[0.257]	[0.045]
Observations	2,278,861	2,278,861	2,278,861

Notes: This table shows the relationship between ancient features and modern population densities, from estimating equation (1). Column 1 reports estimated impacts on grid cell log population density, Column 2 reports estimated impacts on a grid cell having "Urban Density" (log population density > 6), and Column 3 reports impacts on a grid cell having "City Density" (log population density > 9). We measure population density using 2015 population per square kilometer estimates from the GPWv4 model (CIESIN, 2018).

Panel A shows effects of an ancient port site. For comparison, Panel B shows effects of ancient cities in three size categories, using ancient city data from Talbert (2000) and Hanson (2016). In our sample, restricted to 1km-by-1km grid cells within 50km of the coast, there are 10 cities in the 1st category, 101 in the second category, and 480 in the third category.

All estimates include the baseline controls for grid cell characteristics: log distance to the coast, log distance to the nearest major river, latitude, longitude, terrain ruggedness (standard deviation of elevations within the grid cell), and average temperature and precipitation in both January and July. In parentheses are robust standard errors clustered by 1/12-degree-by-1/12-degree groups (roughly 8km-by-8km in the middle of our sample region). For the outcome means, standard deviations are reported in square brackets.

Table 2. Probability of City Density at Distances to Ancient Port

	At 20km (1)	At 40km (2)	Difference: 40km - 20km (3)
Panel A. With Natural Harbor vs. Without (from Figure 6, Panel D)			
Estimated Difference	-0.0042	0.0012	0.0054
	(0.0010)	(0.0006)	(0.0013)
Panel B. With Natural Harbor vs. Log Fit (from Figure 7, Panel D)			
Estimated Deviation from Log Fit	-0.0025	0.0016	0.0040
	(0.0002)	(0.0005)	(0.0005)
Outcome Mean	0.0020	0.0020	0.0020
	[0.0447]	[0.0447]	[0.0447]
Observations	2,278,861	2,278,861	2,278,861

Notes: This table reports a few numbers from Figures 6 and 7, Panel D. Panel A corresponds to Panel D of Figure 6, and Panel B corresponds to Panel D of Figure 7. Column 3 reports the difference between the coefficients in Columns 2 and 1.

Table 3. Estimated Impacts on Ancient Port Grid Cells from Harbor Loss and Nearby Ancient Port Grid Cells Losing Their Natural Harbor

	Modern Port Structure	Ln Population Density	Urban Density	City Density
	(1)	(2)	(3)	(4)
No Harbor	-0.383	-0.269	-0.050	-0.017
	(0.016)	(0.099)	(0.019)	(0.008)
Surrounding Share with No Harbor	-0.039	0.973	0.134	0.041
	(0.039)	(0.225)	(0.044)	(0.020)
Outcome Mean	0.467	4.721	0.267	0.024
	[0.499]	[2.162]	[0.443]	[0.154]
Observations	4,198	4,198	4,198	4,198

Notes: This table shows effects on ancient port grid cells from losing their own natural harbor and nearby ancient port grid cells losing their natural harbor. These coefficients are estimated and reported jointly, following equation 3, for the effect of having no modern natural harbor and "Surrounding Share with No Harbor" that refers to the share of ancient port grid cells within 5-50km that have no modern natural harbor. This sample is restricted to grid cells with an ancient port, within 50km of the coast, that also have at least one other ancient port grid cell within 5-50km.

Column 1 reports effects on having a "Modern Port Structure," which is an indicator for satellite-visible human-made structures to assist the loading and unloading of boats (including a basic pier). Column 2 reports effects on log population density of each grid cell, Column 3 reports effects on "Urban Density" (log population density > 6), and Column 4 reports effects on "City Density" (log population density > 9).

All estimates control for the number of other ancient port grid cells within 5-50km and the baseline controls for grid cell characteristics: log distance to the coast, log distance to the nearest major river, latitude, longitude, terrain ruggedness (standard deviation of elevations within the grid cell), and average temperature and precipitation in both January and July. In parentheses are robust standard errors clustered by 1/12-degree-by-1/12-degree groups (roughly 8km-by-8km in the middle of our sample region). For the outcome means, standard deviations are reported in square brackets.

Online Appendix

Identifying Agglomeration Shadows:
Long-run Evidence from Ancient Ports

Richard Hornbeck
University of Chicago

Guy Michaels
London School of Economics

Ferdinand Rauch
University of Heidelberg

June 2024

A Data Appendix

A.1 Ancient Ports Data

The database on ancient port locations comes from de Graauw (2019). Our use of "ancient" refers to a period around 1,500-3,500 years ago, largely in the Classical World, and limited to the Mediterranean and surrounding areas. The term "port" refers to artificial structures to assist the loading and unloading of boats. De Graauw geo-located these ports based on ancient and modern sources, including the Barrington Atlas, Pleiades dataset, and the Digital Atlas of the Roman Empire (DARE). A large majority of these ancient ports are Greek and Roman. These ancient ports are locations that were used by seafarers sailing over long distances, rather than locations for local fishermen who may have landed their boats on beaches.

The artificial nature of a port distinguishes it from a harbor (or harbour in British English), which is a place where maritime vessels can seek shelter. Almost all of the ancient ports cataloged by de Graauw (2019) are presumed to have been constructed in locations that had a natural harbor. We received from de Graauw a list of 22 known open-water ports from his database that relied more on human-made protections from the sea, which we sometimes exclude from our analysis. We also sometimes exclude 216 locations that de Graauw is less certain of their use as ancient ports.

Some natural harbors have disappeared due to natural processes over the many centuries since those ancient times. The most common of these natural processes was silting and coastal drift, though in some places sinking and land rising also occurred.

We employed the firm Digital Divide Data (DDD) to extract visual information on the modern locations of the ancient ports. We obtained a satellite image for each ancient port location, using Google Maps, and DDD recorded information visible in these images. The main variables constructed this way are indicators for a natural harbor in the vicinity of each ancient port location (within approximately 1km); modern port structures in that location; and whether these modern port structures (where they exist) are extensive structures, as opposed to basic ones (e.g., a simple pier).

A.2 Other Data Sources

We obtain population data from the NASA Center for International Earth Science Information Network (CIESIN, 2018). We use data for 2015, obtained from Version 4, Revision 11 of the Gridded Population of the World dataset (GPWv4) by CIESIN, with robustness analysis using data for 2000 from CIESIN's earlier Global Rural-Urban Mapping Project, Version 1 (CIESIN, 2011). Both of these datasets provide estimates of population density for a grid of 30 arc seconds, a resolution that is slightly finer than our main 1km-by-1km

grid, which we discuss below.

We also use two datasets from the "Global Human Settlement Layer" (GHSL). For data on modern cities, we use the GHS Urban Centre Database, which has coordinates of city centers, total population, and geographic areas in 2015 (Florczyk et al., 2019). These GHSL data capture the location and geographic extent of modern cities, but rely on defined geographic boundaries of cities and so are more dependent on those chosen administrative boundaries as compared to the more-flexible GPWv4 population density data. We also obtain the "GHS population grid" dataset for 2015 population (Schiavina, Freire, and Mac-Manus, 2019), which provides an alternative measure of grid-level population density but also with a focus on defined "built-up" areas.

We use maps from ESRI for the coastline, river locations, and modern country borders (Esri Atlas, 2014; Esri Data and Maps, 2010). We use these maps to assign grid cells to their country and to calculate distance to the coast. An indicator for deserts comes from the NASA Earth Observatory land cover map (NASA Earth Observatory, 2020), and elevation data come from the Global Digital Elevation Model Version 3 (NASA and METI, 2019).

Other data on grid cells' geographic characteristics comes from several sources. We obtain data on temperature and precipitation from the WorldClim 2 Database (Fick and Hijmans, 2017). We use the 10-year averages of temperature and precipitation in January and July. For a small share of cells with missing temperature and precipitation, we compute a distance-weighted measure of the temperature and precipitation of their neighbors using inverse distance weighted (IDW) interpolation. We use data on terrain ruggedness, based on the standard deviation of elevations, from Nunn and Puga (2012). We obtain data on crop suitability from FAO-GAEZ (IIASA/FAO, 2012).[21] We obtain crop suitability data for wheat, barley, olives, cowpeas, white potatoes, and chickpeas. We construct our measure of sea bounty with the Aquamaps data for 15 fish species' suitability (Kaschner et al., 2019), reconstructing the bounty of the sea index in Dalgaard, Knudsen, and Selaya (2020).

We use mapped ancient locations from the Barrington Atlas (Talbert, 2000), using the database of cities compiled by Hanson (2016) based on the Barrington data. These cover the cities of the Roman Empire between 100 B.C. and A.D. 300. For the locations of Roman roads, we use data from the Digital Atlas of Roman and Medieval Civilizations (McCormick et al., 2013).

---

[21]We measure crop suitability as the agro-climatic potential yield of each crop in dry weight kilogram per hectare, with historical data for 1961-1990 from CRUTS32, assuming rain-fed water supply and low input levels.

A.3   Grid Construction

We merge the above datasets into an equal area grid of $1km^2$ cells using the Lambert Azimuthal Equal Area projection, where we place the reference point in the (approximate) center of the Mediterranean at coordinates 39N and 18.5E (following Bakker et al. (2021)). While these grid cells are all $1km^2$ in area, they are only approximately 1km-by-1km squares in two dimensions, and so we measure all distances in the paper using grid cell centroid coordinates and their geodesic distances. By construction, there are no measurable distortions of distance or angle in the vicinity of the reference point. Even at the Western end of the Mediterranean (at Gibraltar), the distance between grid cell centroids deviates less than 2% from 1km.

To construct our sample of ancient ports, we begin with the ancient ports database (de Graauw, 2019), which covers ancient ports around the Mediterranean, the European Atlantic, the Black Sea, the Red Sea, the Gulf of Aden, the Gulf of Oman, the Persian Gulf, and a few nearby coastal areas. Of the 4,561 ancient ports in the de Graauw dataset, we exclude 134 as the cumulative result of three geographic exclusion criteria. First, following exchanges with de Graauw, we exclude a few isolated ancient ports in areas where the coverage is sparse (and most likely incomplete).[22] Second, we exclude ancient ports that are assigned to a broad area, such as "Ireland" or "Corsica", rather than to specific coordinates. Third, since we focus on analyzing coastal areas, we exclude ancient ports that are more than 50km from the coast.[23]

We match each ancient port and Barrington city location to a grid cell, based on its nearest grid cell centroid (up to 1.5km away), to allow for slight imprecision in coastal maps and location coordinates. Due to small differences in coastal boundaries across datasets, for grid cells with an ancient port or Barrington city and missing population density, we use the mean population density of its "king's neighbor" grid cells with non-missing values. Following this adjustment, there are 4,333 ancient ports in grid cells with population density. A small number of grid cells contain multiple ancient ports, such that there are 4,263 grid cells with an ancient port and population density.[24] For Table 1, we use an indicator for that grid cell having any ancient port. For the Figures and Table 2, we classify the grid cell as having a natural harbor if any location within that grid cell has a natural harbor. For

---

[22]This omits four isolated ancient ports along the German, Scandinavian, and Baltic coasts to the east of Amsterdam. We also exclude one isolated port in Iceland. Along the West African Coast, we restrict the analysis to locations from the Canary Islands northwards. Along the East African coast, we exclude ports south of the Gulf of Aden. We include the coast of the Indian Ocean going east until we reach India.

[23]The excluded inland ports were mostly along the Nile and its delta and a few other major rivers.

[24]There are 4,204 grid cells in our sample with one ancient port, 51 grid cells with two ports, 6 grid cells with three ports, 1 grid cell with four ports, and one grid cell with 5 ports, bringing the number of port grid cells to 4,263.

Table 3, similarly, we use an indicator for that grid cell having any modern port structure.

Across our broader sample region, we calculate the distance from each grid cell to its nearest ancient port, with and without a modern natural harbor, and exclude grid cells that are further than 200km from an ancient port. To calculate the distance from each grid cell to the nearest river, coast, and Roman road, we compute the shortest geodesic distance between features and the grid cell centroid.[25] We exclude grid cells more than 50km from the coast. We also restrict the grid cells to modern countries that have at least one ancient port, which means our grid cells follow the coastlines and end at the borders of Netherlands-Germany, India-Pakistan, and Ireland-UK, as well as at the same dividing lines in the Atlantic Maghreb and Somalia.

---

[25]For other data, we overlay the input maps with the grid cells database and take the values that each grid cell centroid falls on.

Appendix References

Bakker, Jan David, Stephan Maurer, Jörn-Steffen Pischke, and Ferdinand Rauch.
2021. "Of Mice and Merchants: Connectedness and the Location of Economic Activity in the
Iron Age." *Review of Economics and Statistics*, 103(4): 652–665.

Center for International Earth Science Information Network (CIESIN). 2011. "Global
Rural-Urban Mapping Project (GRUMPv1): Population Density Grid." Palisades, NY: NASA
Socioeconomic Data and Applications Center. Version 1. Accessed 2021.

Center for International Earth Science Information Network (CIESIN). 2018. "Gridded
Population of the World (GPWv4): Population Density." Palisades, NY: NASA Socioeconomic
Data and Applications Center. Version 4, Revision 11. Accessed 2021.

Dalgaard, Carl-Johan, Anne Sofie B. Knudsen, and Pablo Selaya. 2020. "The Bounty of
the Sea and Long-Run Development." *Journal of Economic Growth*, 25(3): 259–295.

de Graauw, Arthur. 2019. "The Catalogue of Ancient Coastal Settlements, Ports and Harbours."
Accessed 2019. https://www.ancientportsantiques.com/.

Esri Atlas. 2014. "World Boundaries and Places." Redlands, CA: Environmental Systems Research
Institute (ESRI), ArcGIS Living Atlas of the World. Accessed April 2018.

Esri Data and Maps. 2010. "World Major Rivers." Redlands, CA: Environmental Systems Re-
search Institute (ESRI) Mapping Center, ArcGIS Living Atlas of the World. Accessed 2019.

Fick, Stephen E., and Robert J. Hijmans. 2017. "WorldClim 2: New 1km Spatial Resolution
Climate Surfaces for Global Land Areas." International Journal of Climatology 37 (12): 4302-
4315. Accessed January 2020.

**Florczyk, A., C. Corbane, M. Schiavina, M. Pesaresi, L. Maffenini, M. Melchiorri, P.
Politis, F. Sabo, S. Freire, D. Ehrlich, T. Kemper, P. Tommasi, D. Airaghi, and L.
Zanchetta.** 2019. "GHS-UCDB R2019A: GHS Urban Centre Database 2015, Multitemporal and
Multidimensional Attributes." Brussels: European Commission, Joint Research Centre (JRC),
Global Human Settlement Layer (GHSL). Accessed 2021.

Hanson, J.W. 2016. "Cities Database." Oxford: Oxford Roman Economy Project (OXREP).
Version 1.0. Accessed July 2020. http://www.romaneconomy.ox.ac.uk/.

**International Institute for Applied Systems Analysis (IIASA) and Food and Agricul-
ture Organization of the United Nations (FAO).** 2020. "Global Agro-Ecological Zones
(GAEZ)." Laxenburg, Austria: IIASA; Rome: FAO. Version 4.0. Accessed June 2024.

**Kaschner, K., K. Kesner-Reyes, C. Garilao, J. Segschneider, T. Rius-Barile, J. Rees,
and R. Froese.** 2019. "AquaMaps: Predicted Range Maps for Aquatic Species." Accessed May
2024.

McCormick, Michael, Guoping Huang, Giovanni Zambotti, and Jessica Lavash. 2013.
"Roman Road Network." Cambridge, MA: Digital Atlas of Roman and Medieval Civilizations
(DARMC). Version 2008. Accessed September 2019. https://darmc.harvard.edu/.

National Aeronautics and Space Administration (NASA), and Ministry of Economy, Trade, and Industry (METI) of Japan. 2019. "Advanced Spaceborne Thermal Emission and Reflection Radiometer (ASTER) Global Digital Elevation Model Version 3 (GDEM 003)." NASA Earthdata. Accessed June, 2024. https://asterweb.jpl.nasa.gov/gdem.asp.

National Aeronautics and Space Administration (NASA) Earth Observatory. 2020. "Land Cover Classification Map." NASA Earth Observing System Data and Information System (EOSDIS) Land Processes Distributed Active Archive Center. Accessed July 2020. https://earthobservatory.nasa.gov/.

Nunn, Nathan, and Diego Puga. 2012. "Ruggedness: The Blessing of Bad Geography in Africa." *Review of Economics and Statistics*, 94(1): 20–36. Accessed replication data September 2019. https://diegopuga.org/data/rugged/.

Schiavina, Marcello, Sergio Freire, and Kytt MacManus. 2019. "GHS-POP R2019A - GHS Population Grid Multitemporal (1975-2015)." Brussels: European Commission, Joint Research Centre (JRC), Global Human Settlement Layer (GHSL). Accessed 2021.

Talbert, Richard L.A., ed. 2000. *Barrington Atlas of the Greek and Roman World.* Princeton, NJ: Princeton University Press.

Figure A.1. Share of Instances with Cities by Distance and Population Density

Panel A. Medium Density City, or Greater   Panel B. High Density City
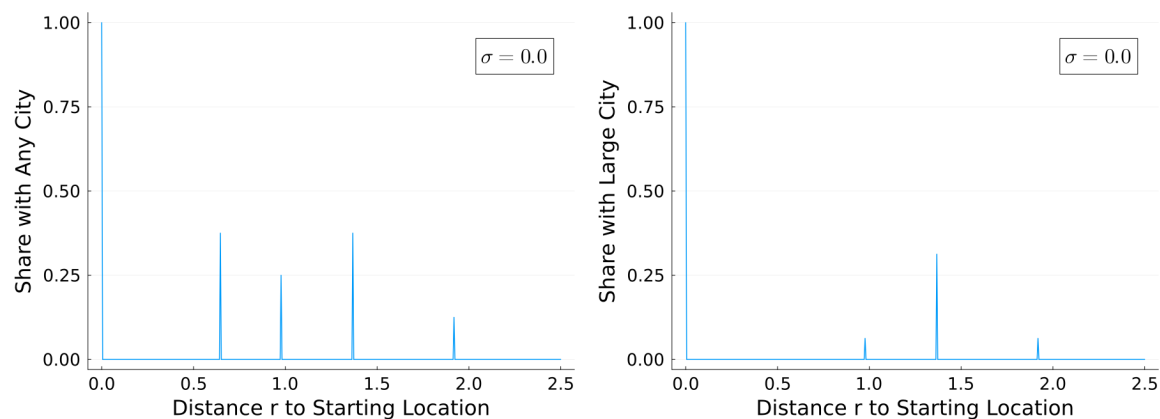
Notes: This figure shows the share of instances in which there is a city at the indicated distance from a starting city, as modeled for the 16 aggregate population parameter values in Fujita, Krugman, and Mori (1999). Panel A shows the share of instances with a city of medium density, defined as a city with log population density > 2, where location is binned to the nearest 0.005. Panel B shows the share of instances with a city of high density, defined as a city with log population density > 3.

Figure A.2. Share of Instances with Cities by Distance and Population Density, with Increasing Spatial Noise

Panel A. Medium Density City, Low Noise
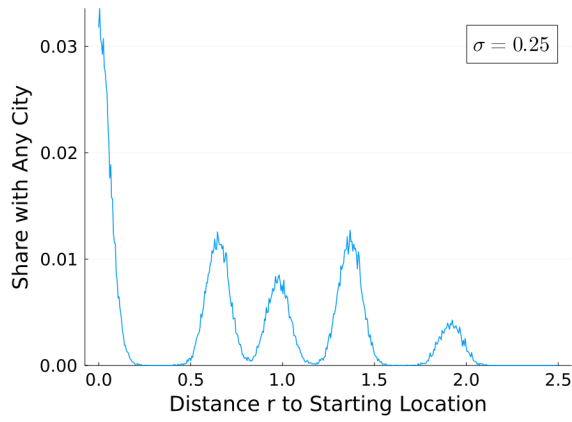
Panel B. High Density City, Low Noise
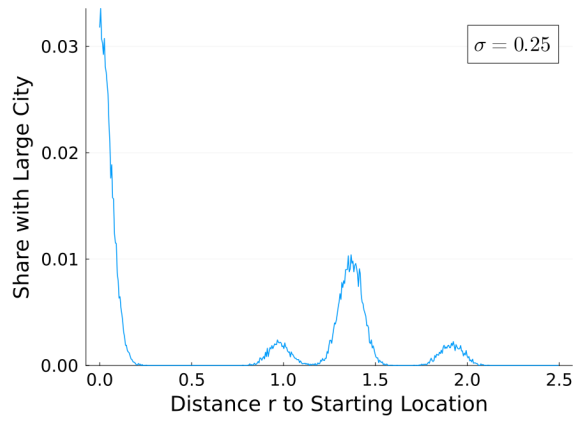
Panel C. Medium Density City, Medium Noise
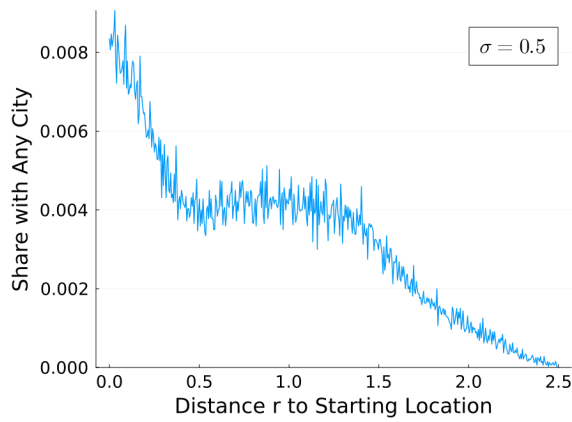
Panel D. High Density City, Medium Noise
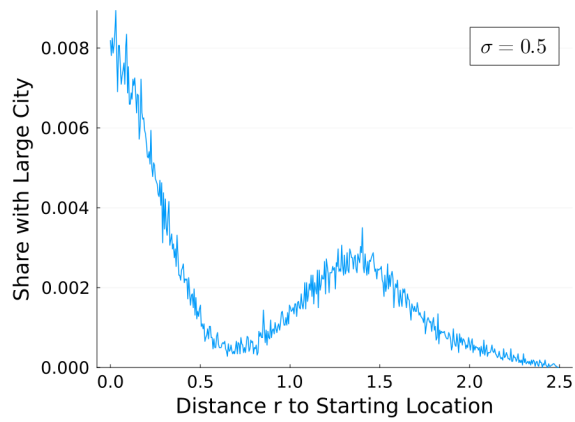
Panel E. Medium Density City, High Noise
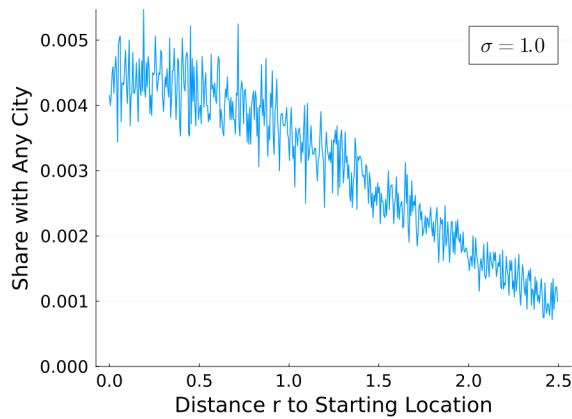
Panel F. High Density City, High Noise
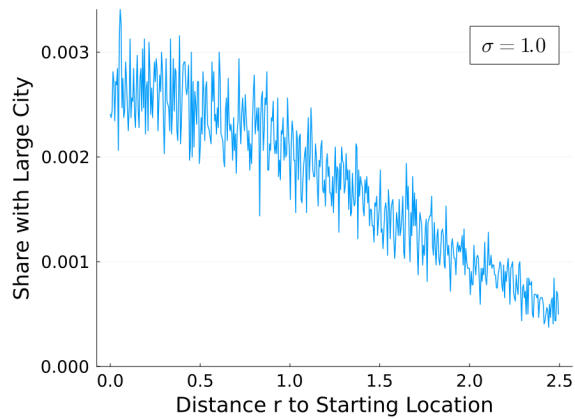
Notes: Each panel reports simulations from Figure A.1, with increasing spatial noise in the fixed starting city's location (at distance zero in Figure A.1): "Low Noise" (standard deviation of 0.25); "Medium Noise" (standard deviation of 0.5); and "High Noise" (standard deviation of 1.0).

Figure A.3. Share of Instances with Cities by Distance and Population Density: Medium versus High Noise

Panel A. Medium Density City, Medium and High Noise

Panel B. High Density City, Medium and High Noise
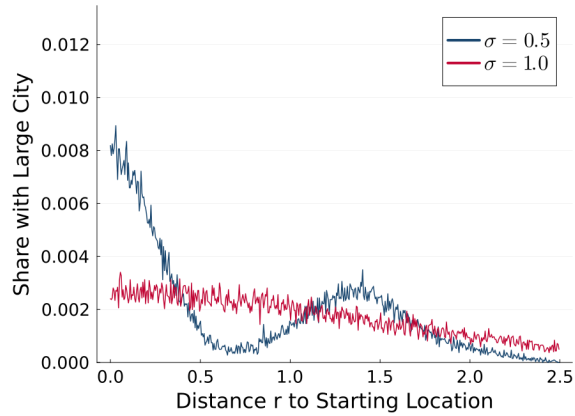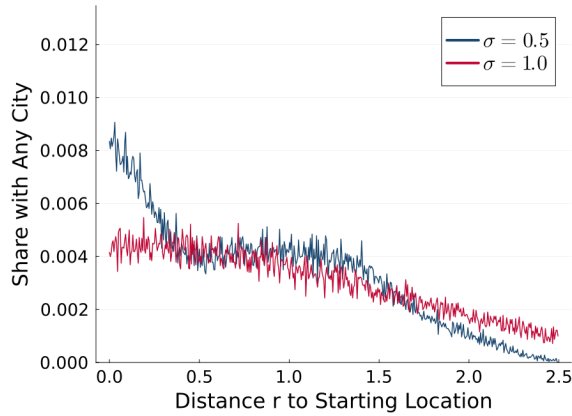
Panel C. Medium Density City, Difference between Medium and High Noise
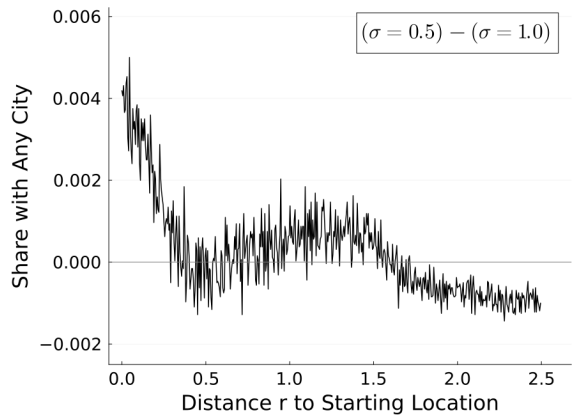
Panel D. High Density City, Difference between Medium and High Noise
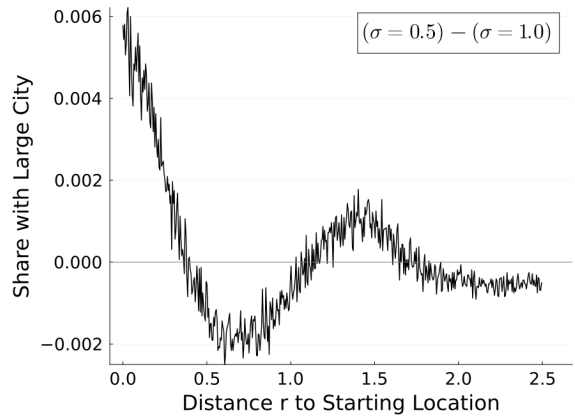
Notes: This figure compares "Medium Noise" and "High Noise" results from the simulations in Figure A.2. Panels A and B show simulations with Medium and High Noise on the same plot, and Panels C and D show the difference in probabilities (Medium Noise minus High Noise).

Figure A.4. Number of Grid Cells by Distance to Nearest Ancient Port, by Modern Harbor Type

Panel A. Distance to Nearest Ancient Port with Harbor
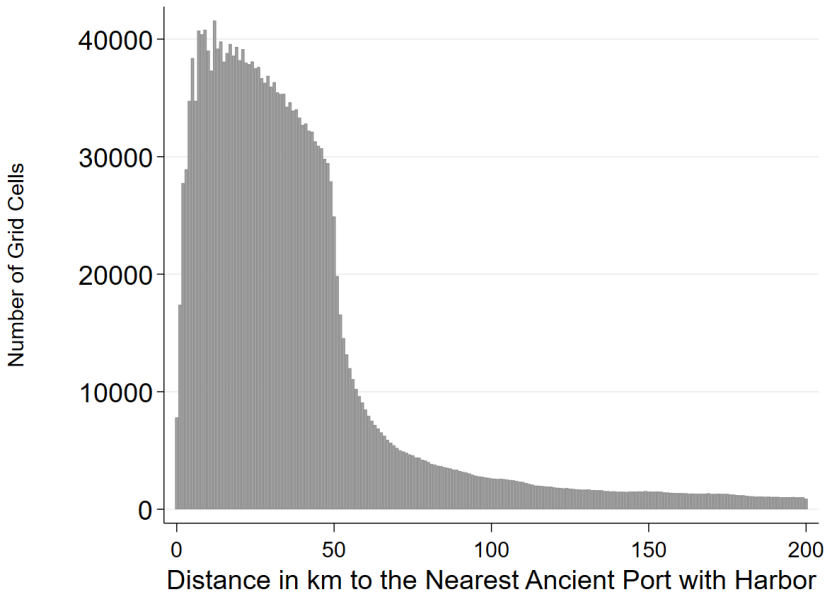
Panel B. Distance to Nearest Ancient Port without Harbor
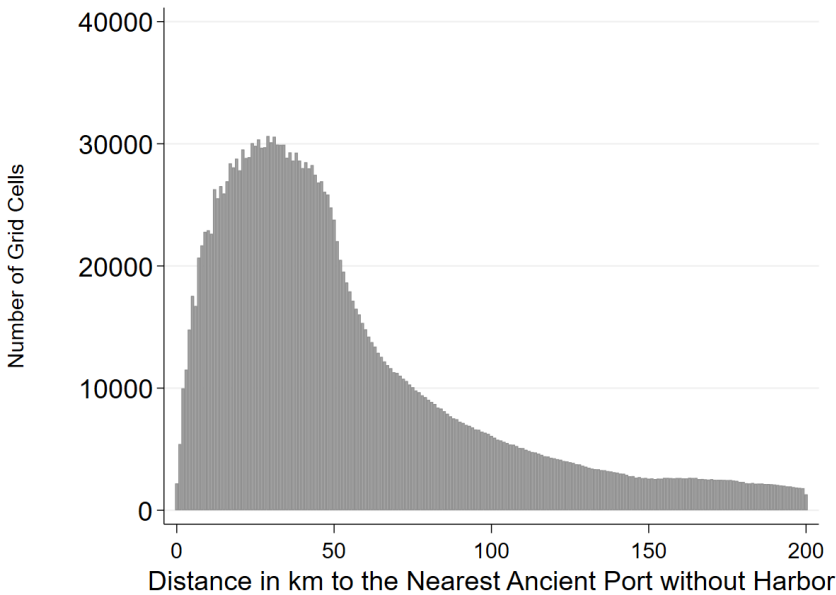
Notes: This figure shows the number of grid cells by distance to nearest ancient port. For each integer kilometer, Panel A shows the number of grid cells at that nearest distance from an ancient port with a natural harbor in the modern era, and Panel B shows the number of grid cells at that distance from a port without a natural harbor in the modern era. We classify a location as having a natural harbor in the modern era if at least one ancient port location at that grid cell is classified as having a natural harbor using satellite imagery. Our sample is restricted to grid cells within 200km of an ancient port, and truncated from this figure are: 2.8% of grid cells that are more than 200km from an ancient port with a modern harbor, and 5.4% of grid cells are more than 200km from an ancient port without a modern harbor.

Figure A.5. Impacts on Probability of City Density, Robustness to Additional Geographic Characteristics
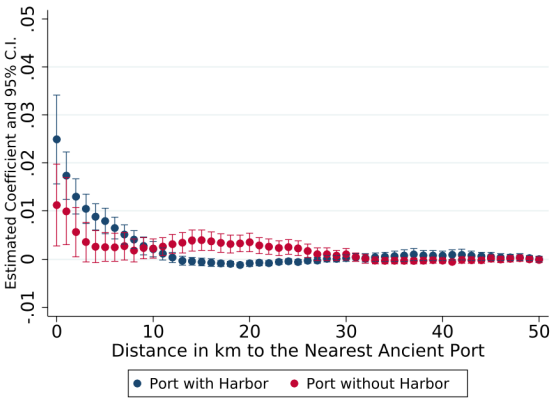
Panel A. Probability of City Density

Panel B. Probability of City Density
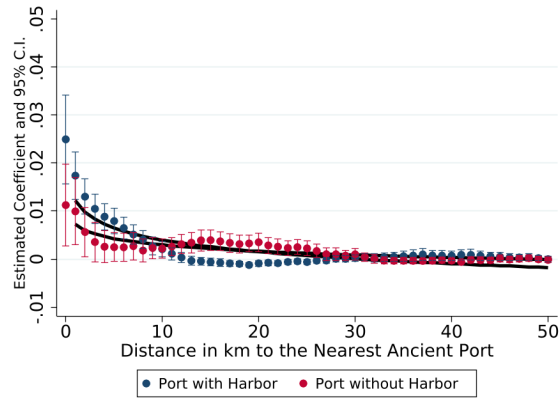
Panel C. Differences for City Density
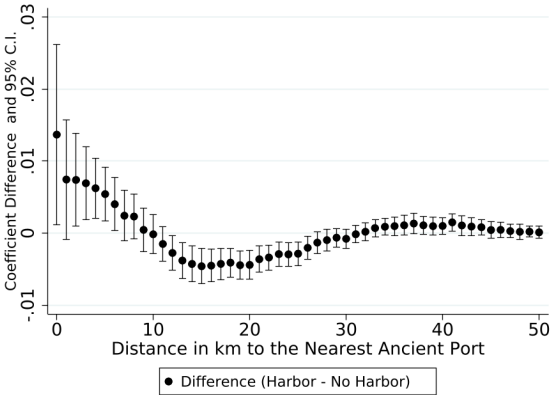
Panel D. City, Difference from Log Fit
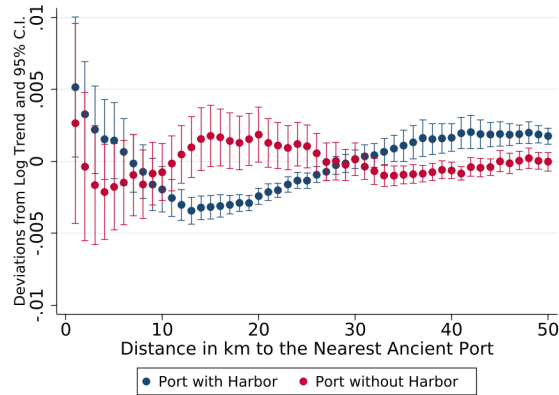
Notes: This figure reproduces estimates from Figures 6 and 7 with additional geographic controls for grid cell characteristics: suitability for potatoes, wheat, barley, cowpeas, olives, and chickpeas; sea bounty; an indicator for desert cell; an indicator for being on an island; elevation; log distance to river mouth; sea bounty interacted within being 2km, 5km, and 10km of the coast; indicators for being within 2km, 5km, and 10km of a coast, a major river, and a river mouth. Panels A and B correspond to Figure 6, Panels B and D. Panels B and D correspond to Figure 7, Panels B and D.

Figure A.6. Impacts on Probability of City Density, Robustness to Excluding Islands

Panel A. Probability of City Density
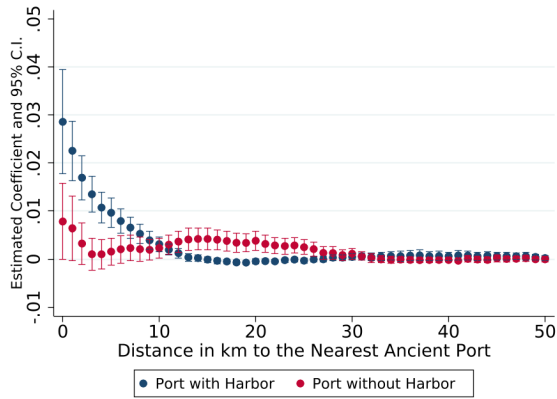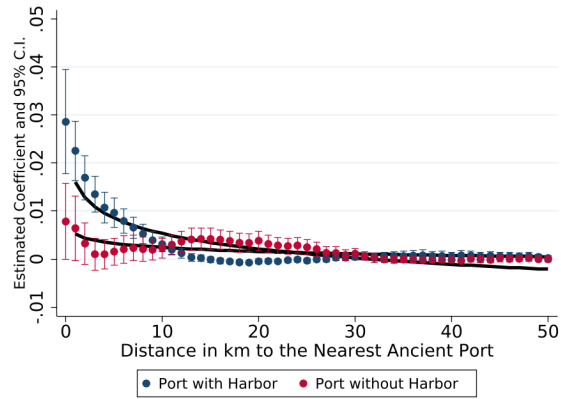
Panel B. Probability of City Density

Panel C. Differences for City Density
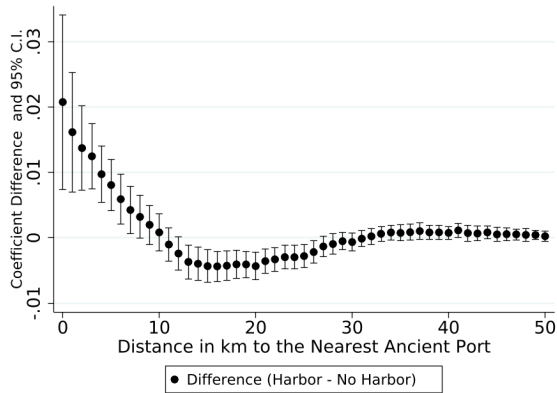
Panel D. City, Difference from Log Fit
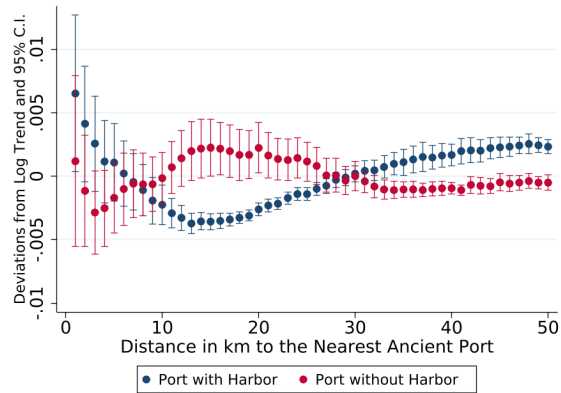
Notes: This figure reproduces estimates from Figures 6 and 7, removing all grid cells on an island smaller than 2,500 square kilometers. Panels A and B correspond to Figure 6, Panels B and D. Panels B and D correspond to Figure 7, Panels B and D.

Figure A.7. Impacts on Probability of City Density, Robustness to Excluding "Potential Ancient Harbors"

Panel A. Probability of City Density
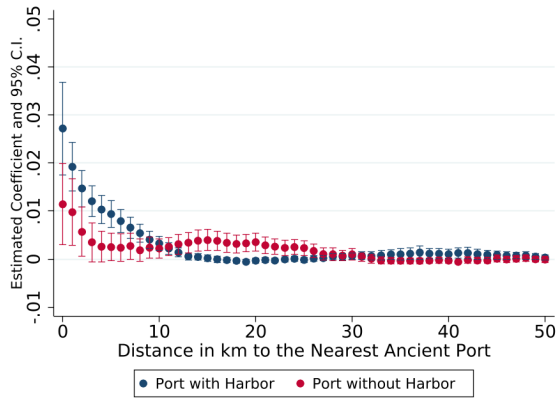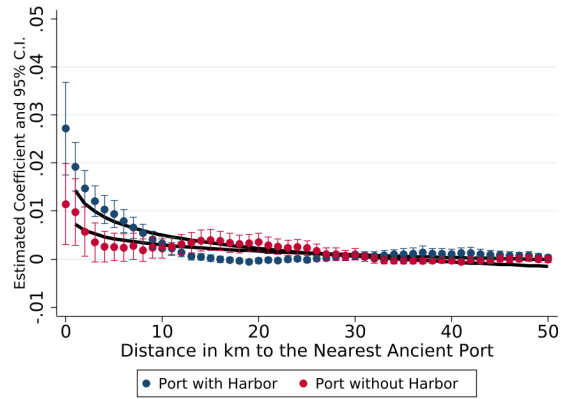
Panel B. Probability of City Density

Panel C. Differences for City Density
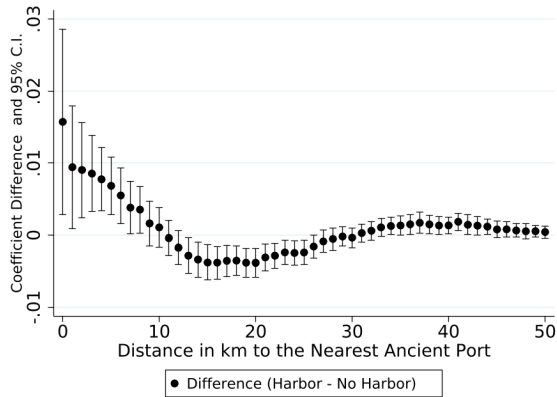
Panel D. City, Difference from Log Fit
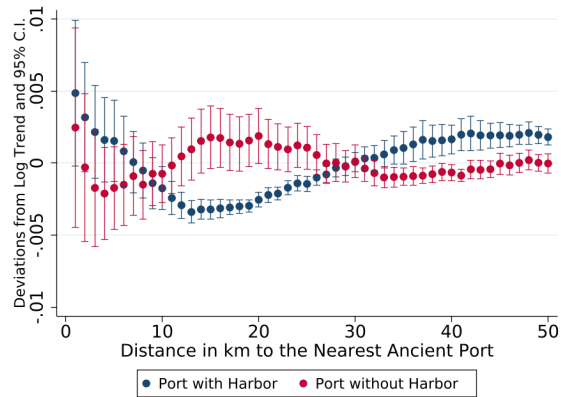
Notes: This figure reproduces estimates from Figures 6 and 7, excluding 216 locations where de Graauw is less certain of their use as ancient ports. Panels A and B correspond to Figure 6, Panels B and D. Panels B and D correspond to Figure 7, Panels B and D.

Figure A.8. Impacts on Probability of City Density, Robustness to Ancient Economic Characteristics
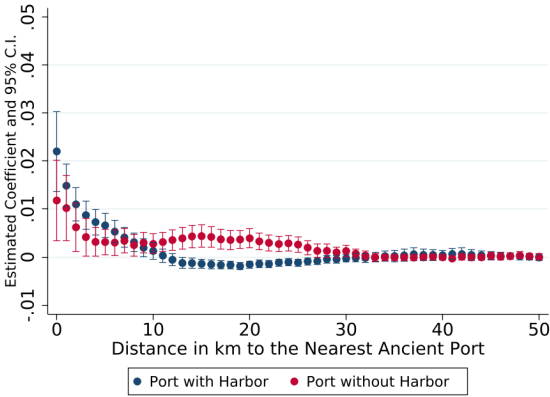
Panel A. Probability of City Density

Panel B. Probability of City Density
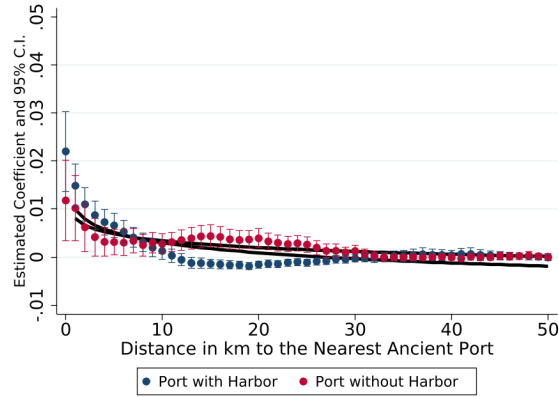
Panel C. Differences for City Density
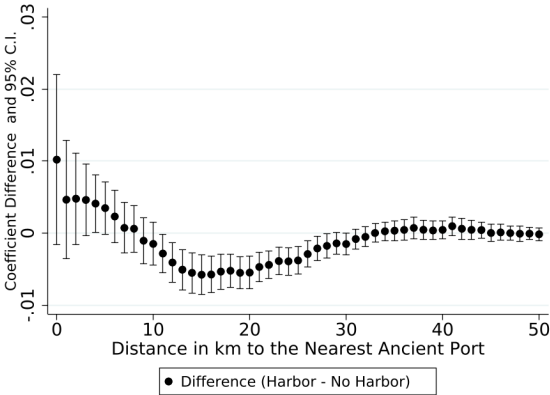
Panel D. City, Difference from Log Fit
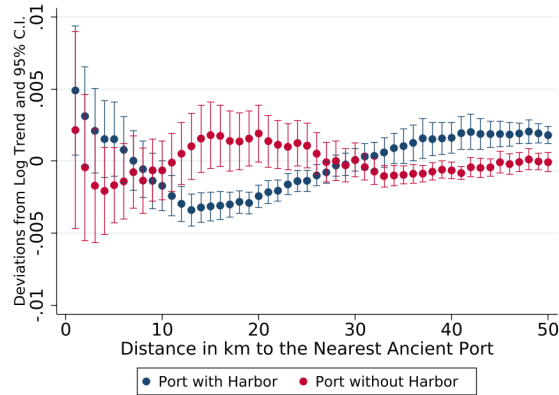
Notes: This figure reproduces estimates from Figures 6 and 7, with additional controls for grid cell characteristics in the ancient era: log distance to nearest Roman road and log distance to each Barrington 1 city (Talbert, 2000; Hanson, 2016): Aelia Capitolina (Jerusalem); Alexandria; Antioch (Antakya); Athens; Byzantium (Istanbul); Carthage; Córdoba; Corinth; Leptis Magna; Lugdunum (Lyon); Mediolanum (Milan); Rome; Tarraco (Tarragona); and Thessalonica. Panels A and B correspond to Figure 6, Panels B and D. Panels B and D correspond to Figure 7, Panels B and D.

Figure A.9. Impacts on Probability of City Density, Robustness to Excluding Ancient Open-Water Ports
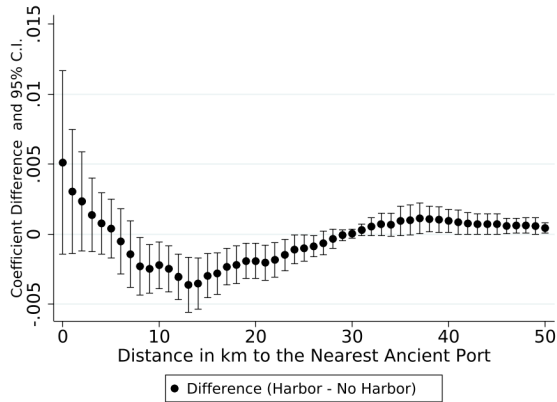
Panel A. Probability of City Density
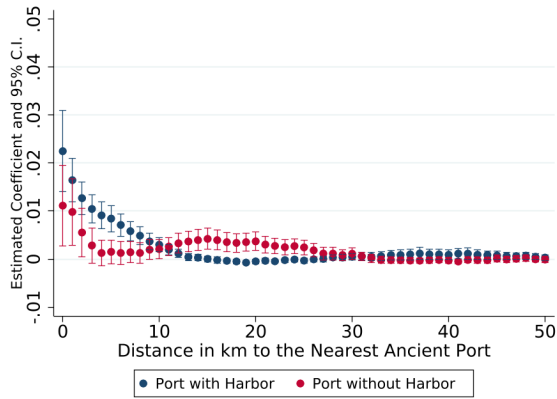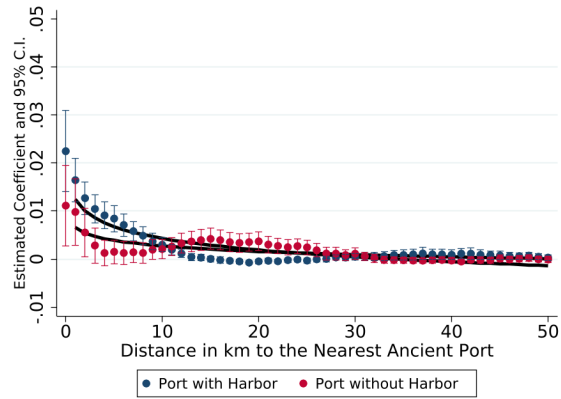
Panel B. Probability of City Density

Panel C. Differences for City Density
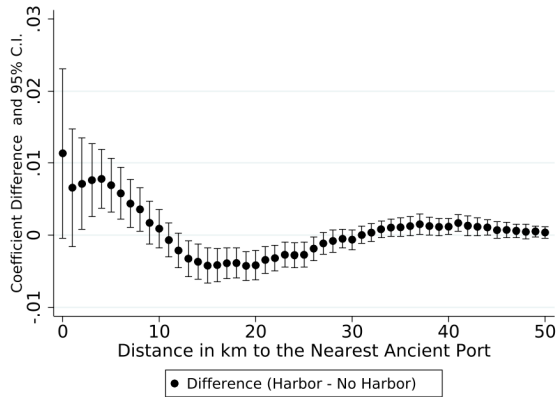
Panel D. City, Difference from Log Fit
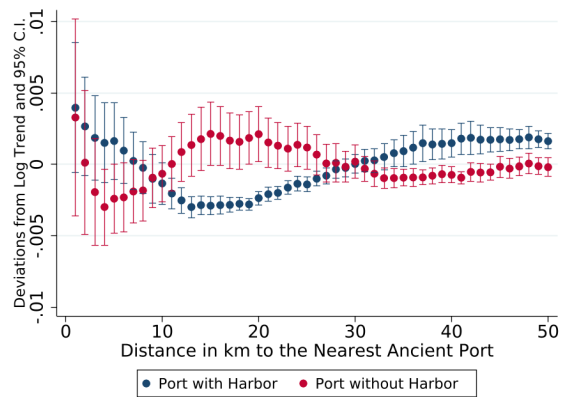
Notes: This figure reproduces estimates from Figures 6 and 7, removing all grid cells within 20km of 22 ancient open-water ports (those that are known to have relied on human-made protections from the sea). Panels A and B correspond to Figure 6, Panels B and D. Panels B and D correspond to Figure 7, Panels B and D.

Figure A.10. Impacts on Probability of City Density, Robustness to Excluding Barrington 1 Cities
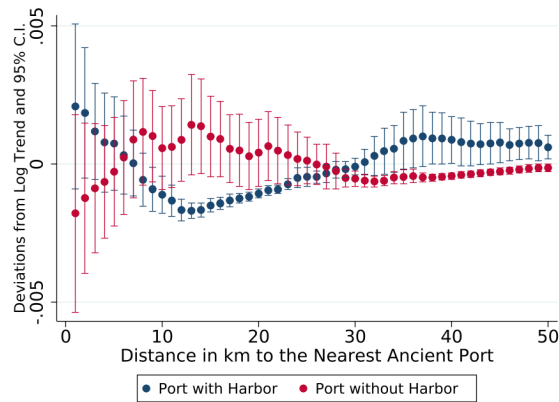
Panel A. Probability of City Density
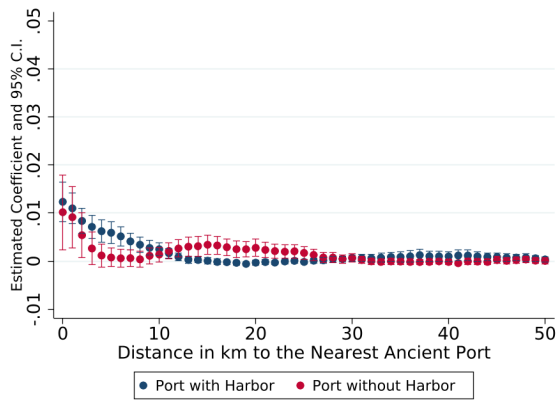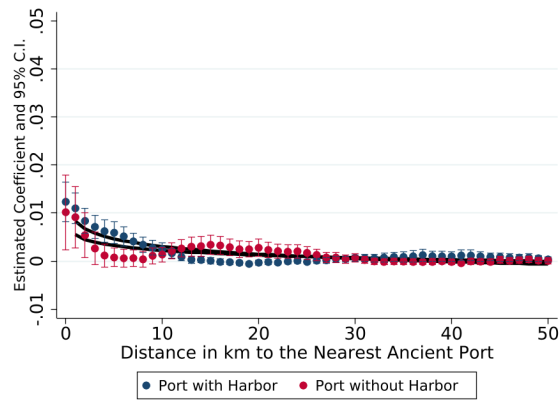
Panel B. Probability of City Density

Panel C. Differences for City Density
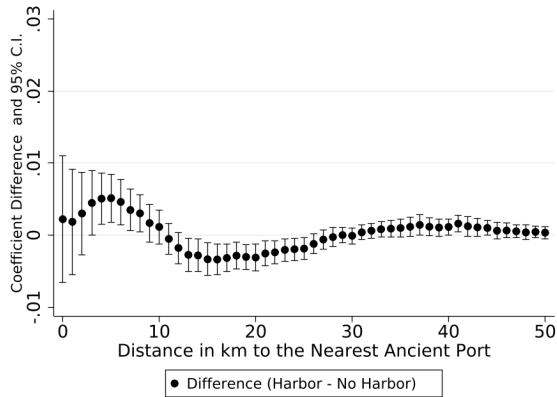
Panel D. City, Difference from Log Fit
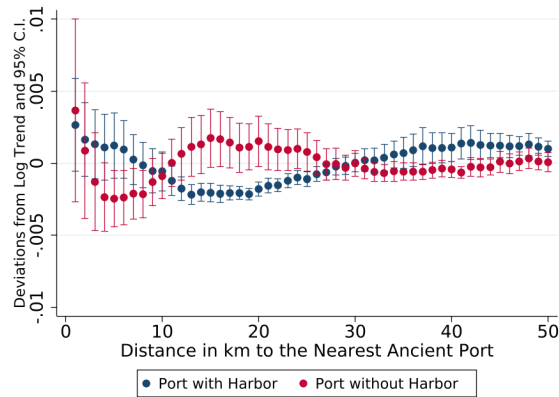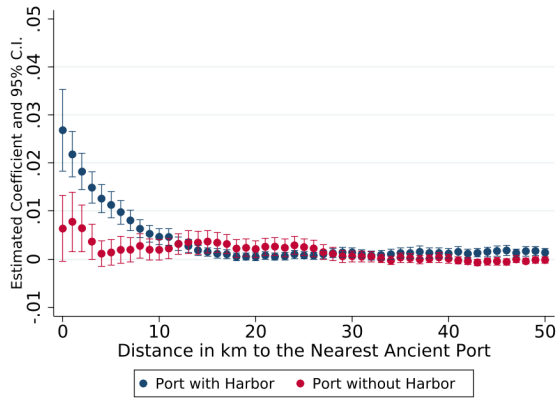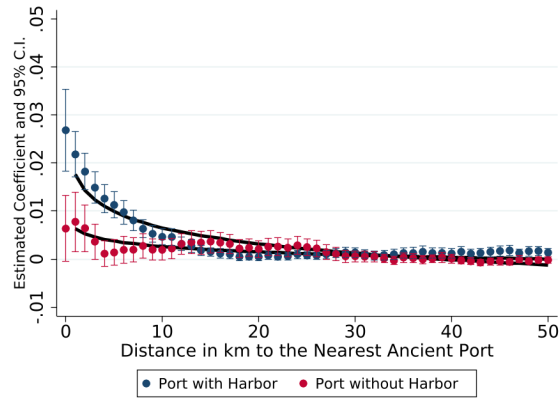

Notes: This figure reproduces estimates from Figures 6 and 7, removing all grid cells within 20km of 14 Barrington 1 Cities (Talbert, 2000; Hanson, 2016): Aelia Capitolina (Jerusalem); Alexandria; Antioch (Antakya); Athens; Byzantium (Istanbul); Carthage; Córdoba; Corinth; Leptis Magna; Lugdunum (Lyon); Mediolanum (Milan); Rome; Tarraco (Tarragona); and Thessalonica. Panels A and B correspond to Figure 6, Panels B and D. Panels B and D correspond to Figure 7, Panels B and D.

Figure A.11. Impacts on Probability of City Density, Robustness to 2-Degree by 2-Degree Fixed Effects
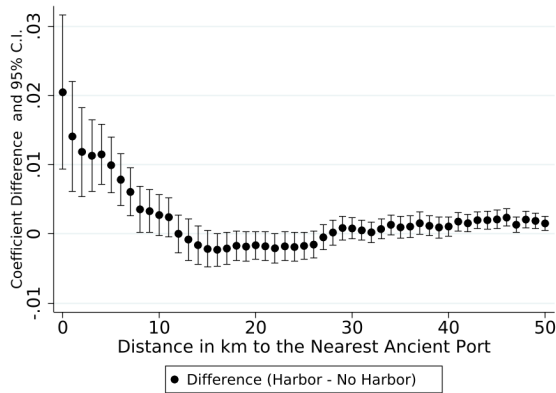
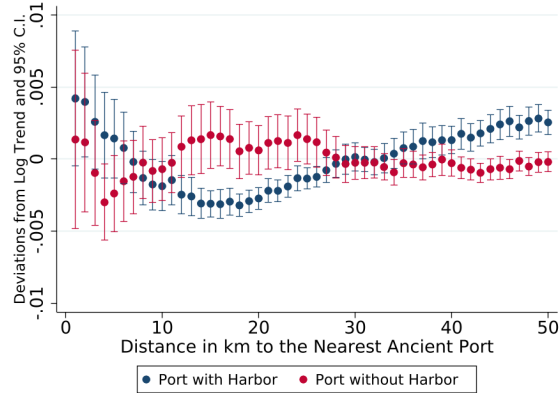Panel A. Probability of City Density
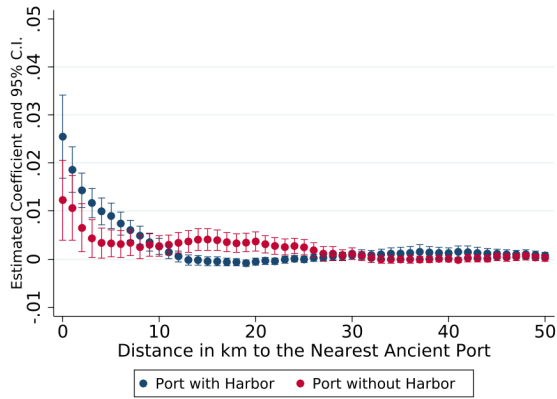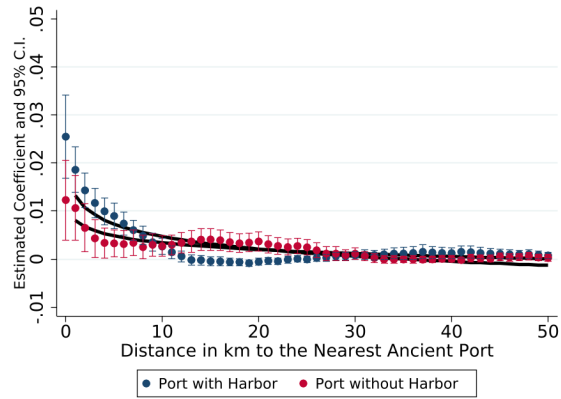
Panel B. Probability of City Density

Panel C. Differences for City Density
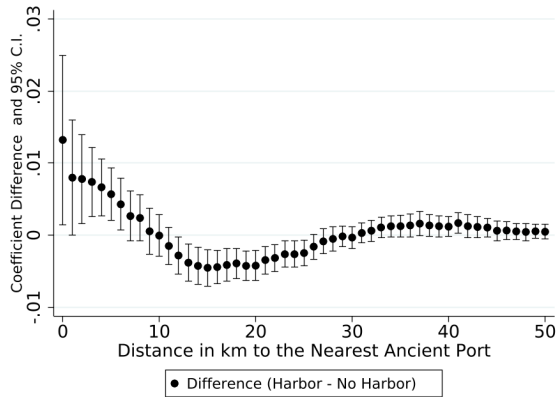
Panel D. City, Difference from Log Fit
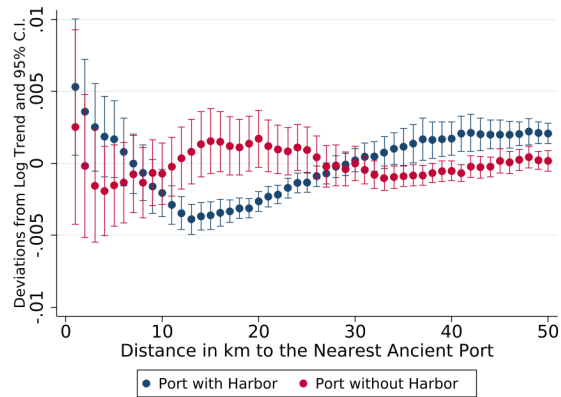
Notes: This figure reproduces estimates from Figures 6 and 7, adding fixed effects for 2-degree by 2-degree grid cell groupings. Panels A and B correspond to Figure 6, Panels B and D. Panels B and D correspond to Figure 7, Panels B and D.

17

Figure A.12. Impacts on Probability of City Density, Robustness to Modern Country Fixed Effects

Panel A. Probability of City Density
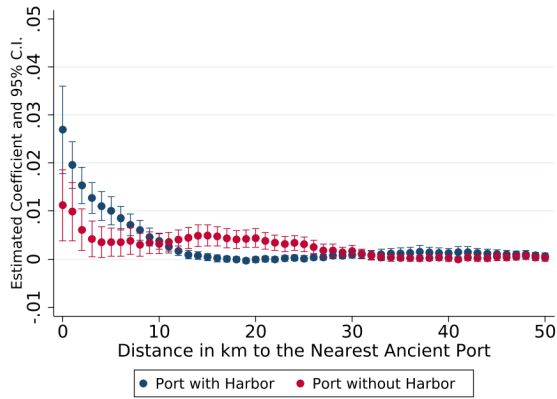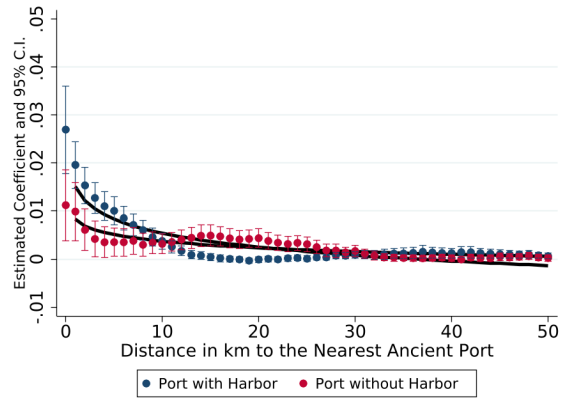
Panel B. Probability of City Density
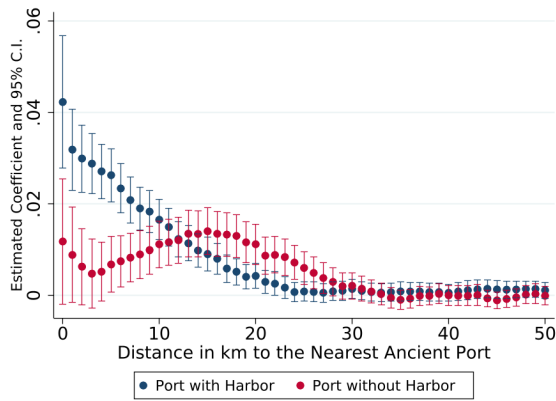

Panel C. Differences for City Density
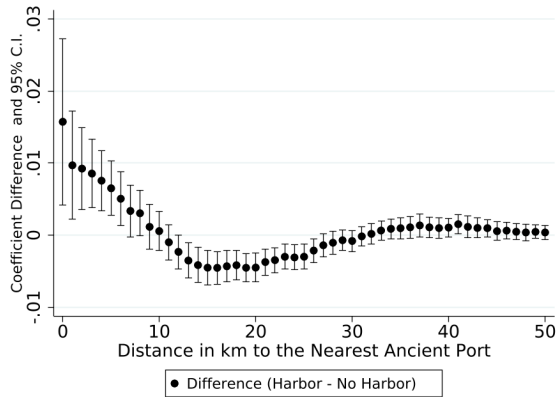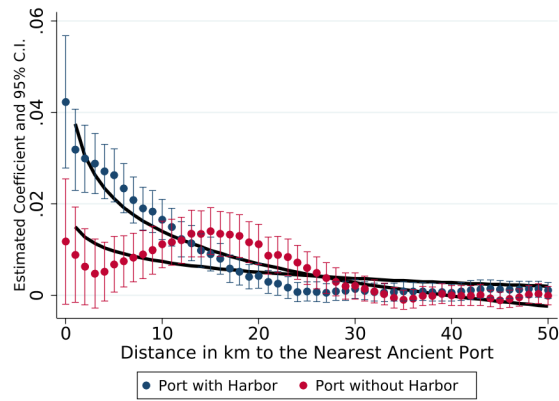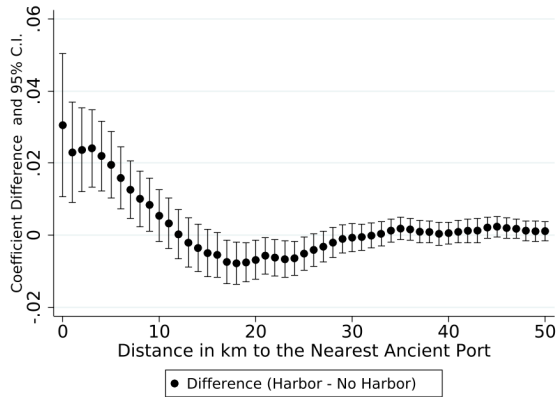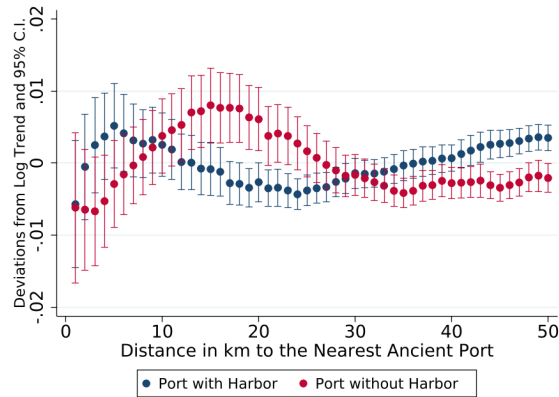
Panel D. City, Difference from Log Fit
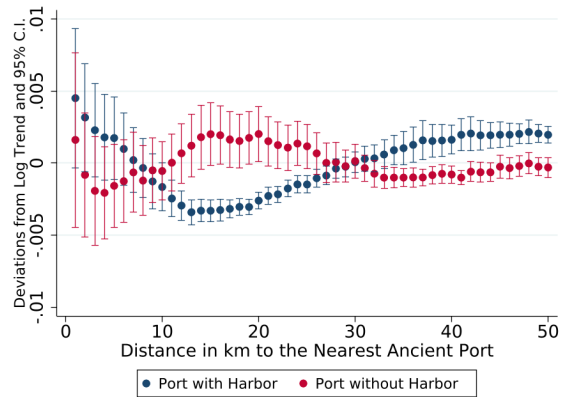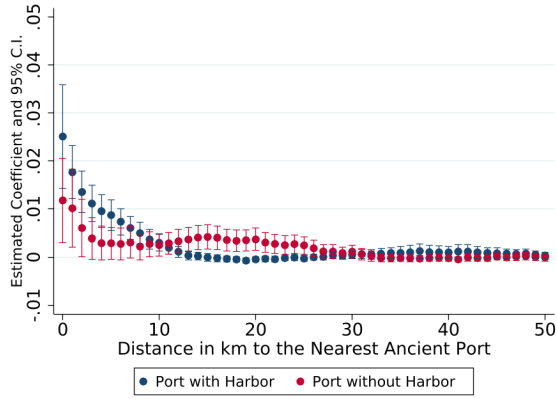

Notes: This figure reproduces estimates from Figures 6 and 7, adding fixed effects for present-day country. Panels A and B correspond to Figure 6, Panels B and D. Panels B and D correspond to Figure 7, Panels B and D.

Figure A.13. Coefficient Differences, Across Population Density Thresholds
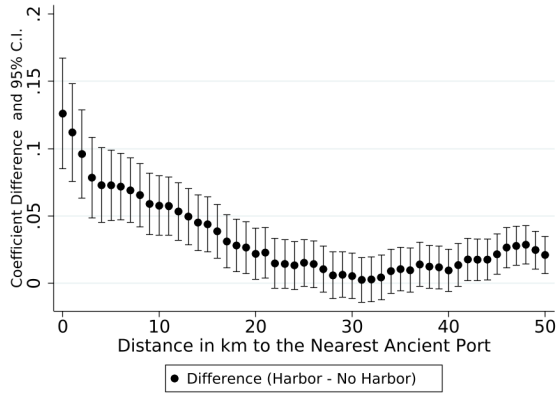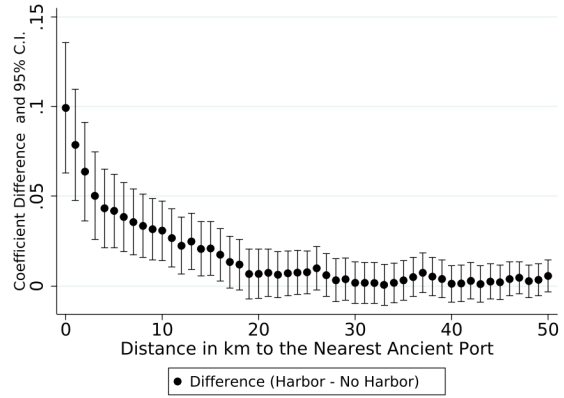
Panel A. Ln(Density) > 5

Panel B. Ln(Density) > 6
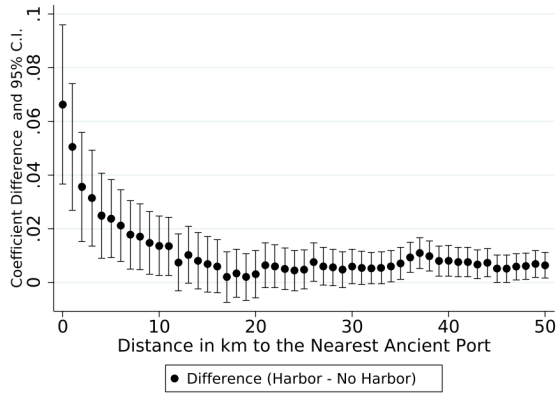
Panel C. Ln(Density) > 7
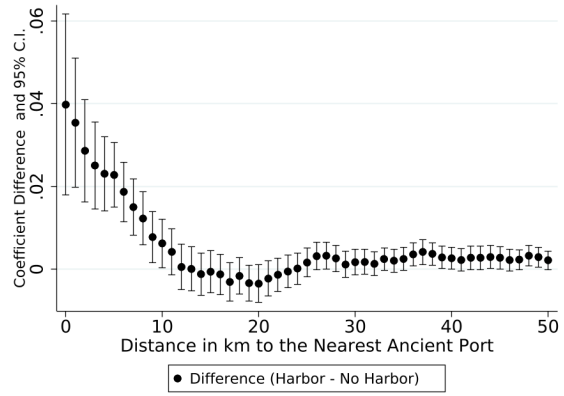
Panel D. Ln(Density) > 8
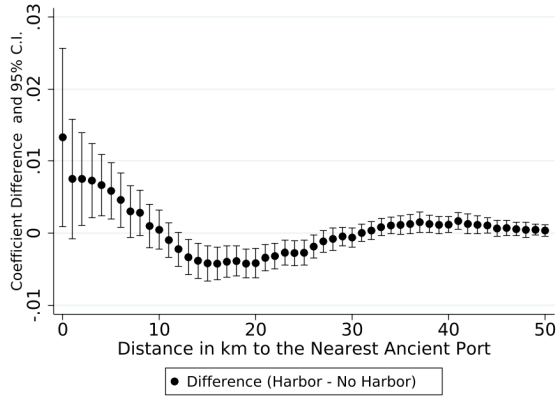
Panel E. Ln(Density) > 9

Panel F. Ln(Density) > 10
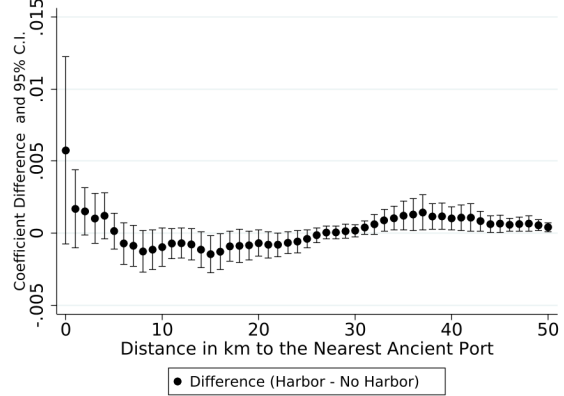
Notes: This figure shows the differences between the harbor and no harbor estimates of the effect of distance on different log population density thresholds. Panels B and E match Panels C and D of Figure 6, and the other panels report results for alternate log population density cutoff values from 5 to 10.

Figure A.14. Differences from Log Fit, Across Population Density Thresholds
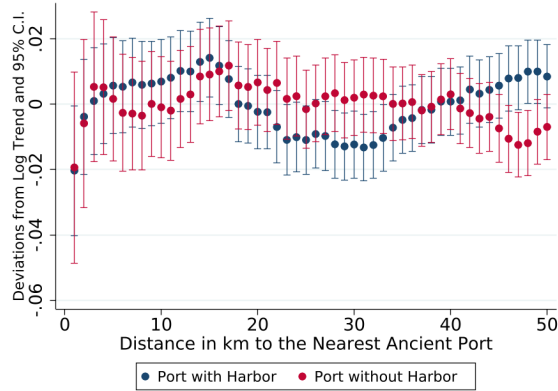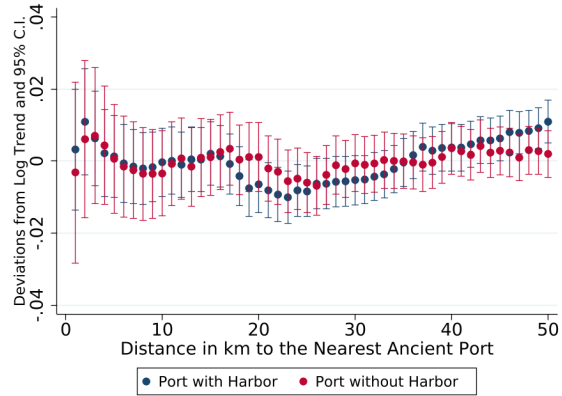
Panel A. Ln(Density) > 5   Panel B. Ln(Density) > 6
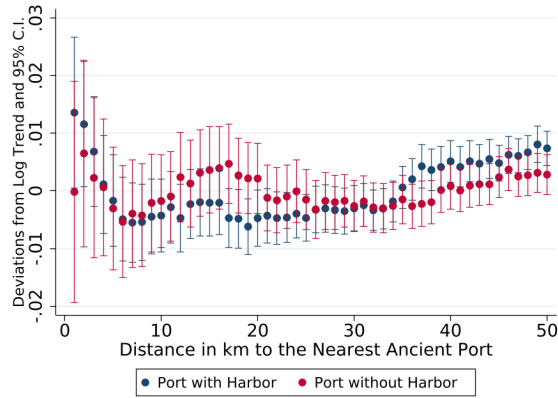
Panel C. Ln(Density) > 7   Panel D. Ln(Density) > 8
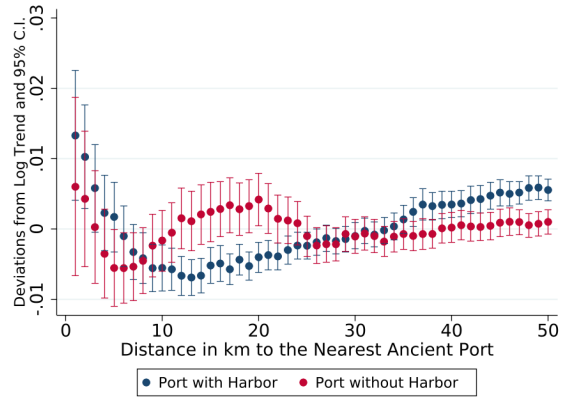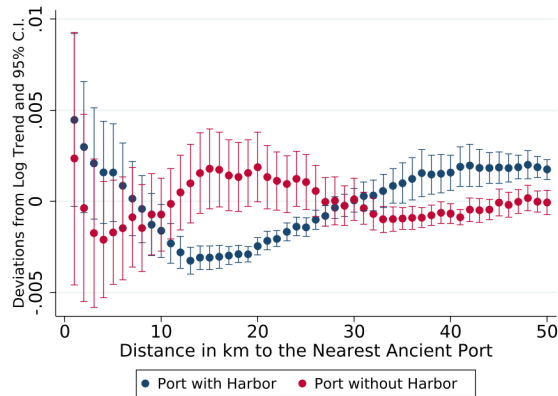
Panel E. Ln(Density) > 9   Panel F. Ln(Density) > 10
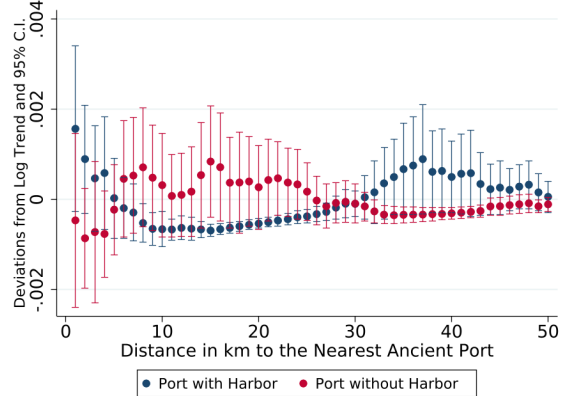
Notes: This figure shows differences between the log fit and the estimated effects of distance on different log population density levels, for distances to ports both with and without modern harbors. Panels B and E match Panels C and D of Figure 7, and the other panels report results for alternate log population density cutoff values from 5 to 10.

20

Figure A.15. Impacts on Probability of City Density, Robustness to 2000 GRUMP Data

Panel A. Probability of City Density
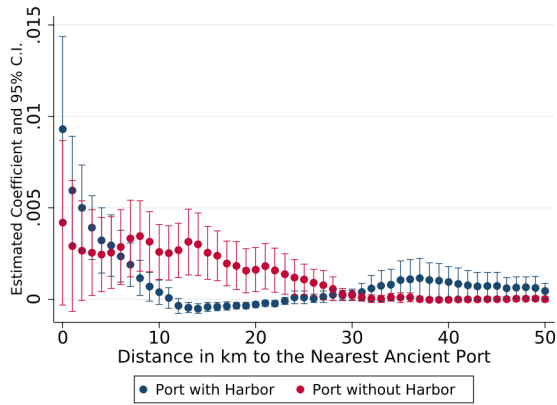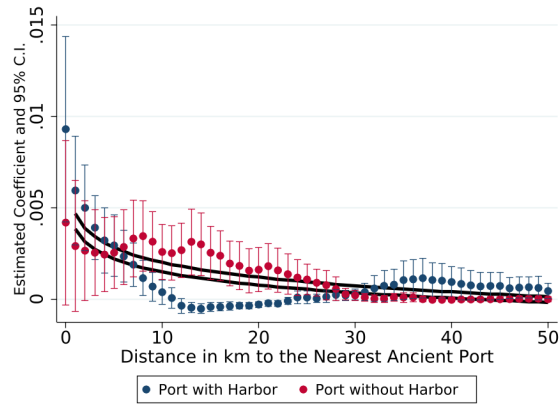
Panel B. Probability of City Density

Panel C. Differences for City Density

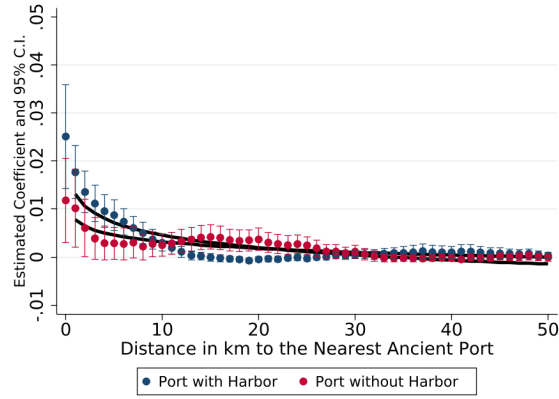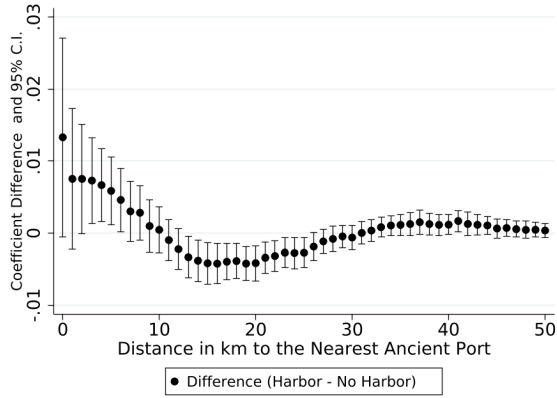Panel D. City, Difference from Log Fit

Notes: This figure reproduces estimates from Figures 6 and 7, using population per square kilometer estimates for 2000 from the earlier GRUMP model (CIESIN, 2011). Panels A and B correspond to Figure 6, Panels B and D. Panels B and D correspond to Figure 7, Panels B and D.

Figure A.16. Impacts on Probability of City Density, Robustness to GHSL Density Data

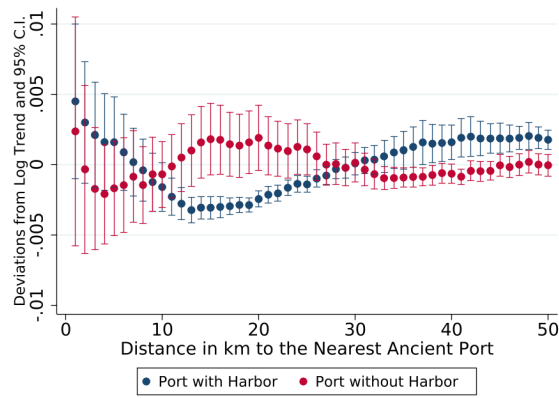Panel A. Probability of City Density

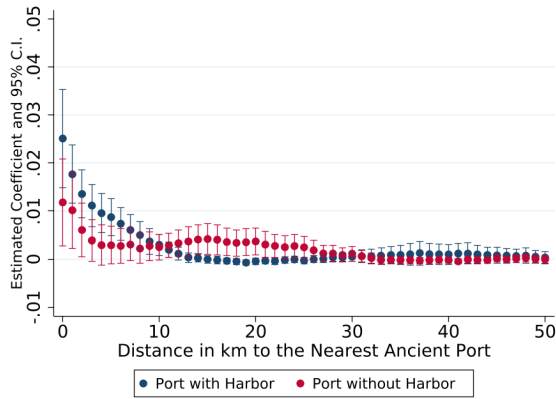Panel B. Probability of City Density

Panel C. Differences for City Density
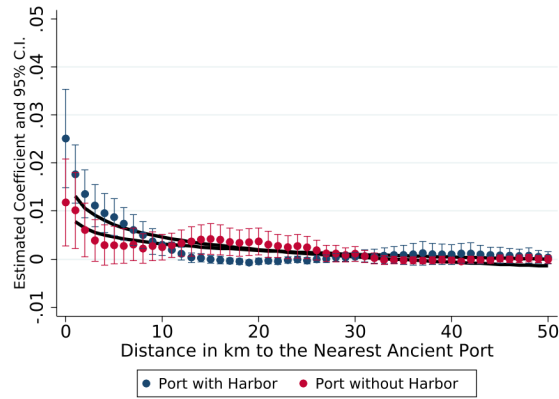
Panel D. City, Difference from Log Fit

Notes: This figure reproduces estimates from Figures 6 and 7, using population per square kilometer estimates for 2015 from the GHSL-POP model (Schiavina, Freire, and MacManus, 2019). Panels A and B correspond to Figure 6, Panels B and D. Panels B and D correspond to Figure 7, Panels B and D.

Figure A.17. Impacts on Probability of City Density, Robustness to GHSL City Location Data
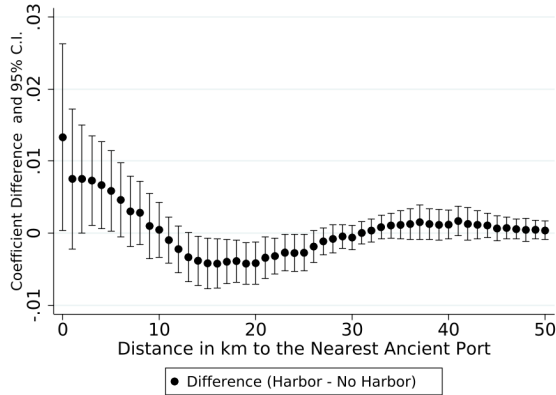
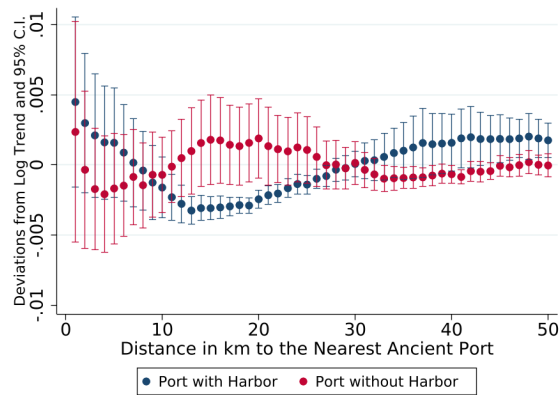Panel A. Probability of City Density

Panel B. Probability of City Density

Panel C. Differences for City Density

Panel D. City, Difference from Log Fit

Notes: This figure reproduces estimates from Figures 6 and 7, using an alternative outcome of being within a city. We define a grid cell as within a city if it is within the "radius" ($\sqrt{\text{Area}/\pi}$) of a city center location, for cities over 500,000 people, using 2015 area and population estimates from the GHS Urban Centre Database (Florczyk et al., 2019). Panels A and B correspond to Figure 6, Panels B and D. Panels B and D correspond to Figure 7, Panels B and D.

Figure A.18. Impacts on Probability of City Density, Robustness to Two-Way Clustered Standard Errors with Shifted Clusters

Panel A. Probability of City Density

Panel B. Probability of City Density
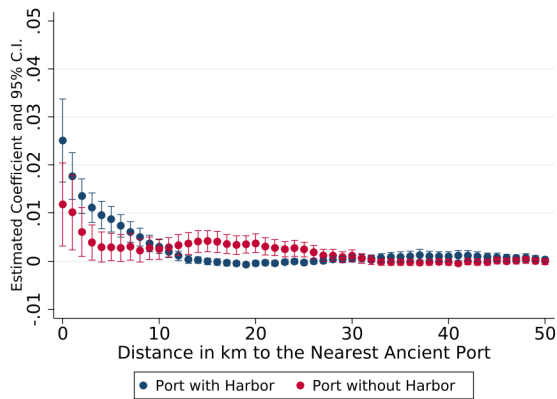

Panel C. Differences for City Density

Panel D. City, Difference from Log Fit

Notes: This figure reproduces estimates from Figures 6 and 7, with the estimation of standard errors using two-way clusters with additional clusters shifted by 1/24 degree latitude and 1/24 degree longitude from baseline. Panels A and B correspond to Figure 6, Panels B and D. Panels B and D correspond to Figure 7, Panels B and D.

Figure A.19. Impacts on Probability of City Density, Robustness to Clustering by 1/4-Degree by 1/4-Degree Squares

Panel A. Probability of City Density

Panel B. Probability of City Density

Panel C. Differences for City Density

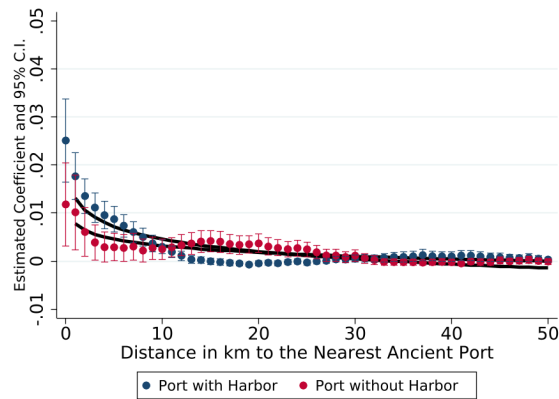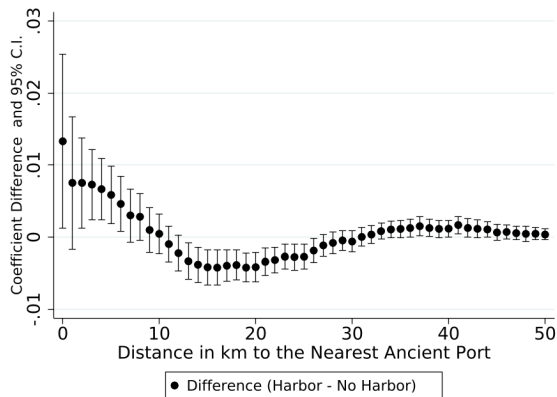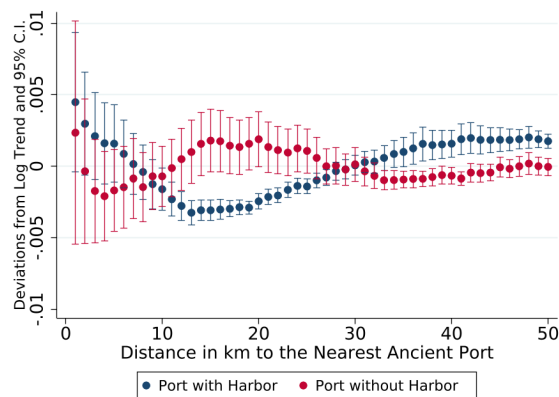Panel D. City, Difference from Log Fit

Notes: This figure reproduces estimates from Figures 6 and 7, with standard errors clustered instead at the level of 1/4-degree-by-1/4-degree groups. Panels A and B correspond to Figure 6, Panels B and D. Panels B and D correspond to Figure 7, Panels B and D.

Figure A.20. Impacts on Probability of City Density, Robustness to Using Conley Standard Errors with 4km Cutoff

Panel A. Probability of City Density

Panel B. Probability of City Density
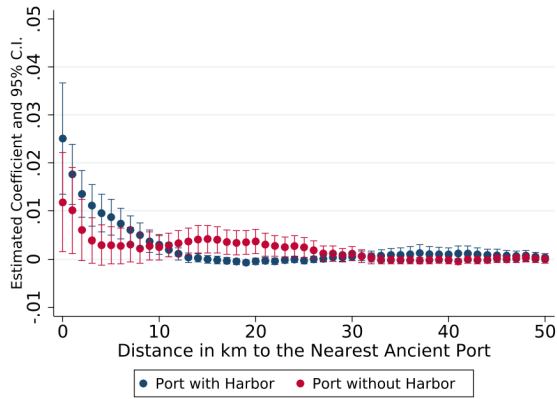
Panel C. Differences for City Density

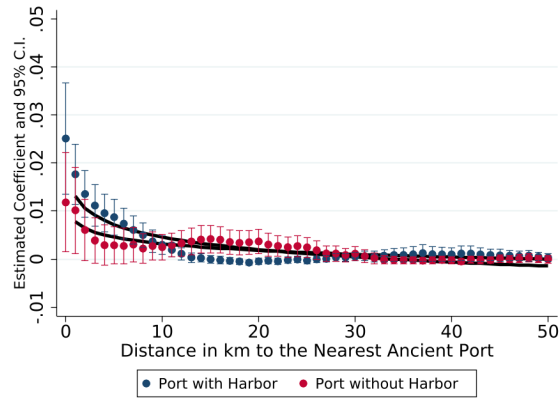Panel D. City, Difference from Log Fit

Notes: This figure reproduces estimates from Figures 6 and 7, instead using Conley standard errors (Conley, 1999) that allow for spatial correlation that declines linearly in distance up to a 4km cutoff. By comparison, the median size city in our sample has a radius of 4km. Panels A and B correspond to Figure 6, Panels B and D. Panels B and D correspond to Figure 7, Panels B and D.

Figure A.21. Impacts on Probability of City Density, Robustness to Using Conley Standard Errors with 8km Cutoff
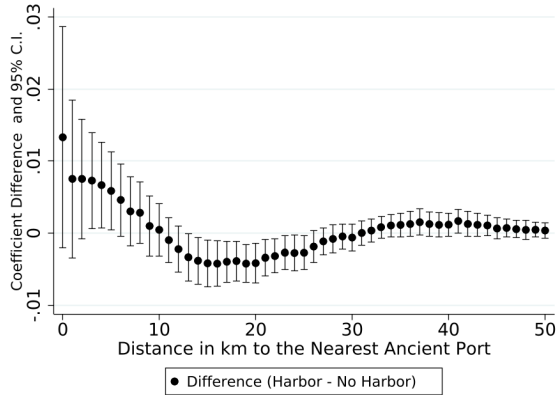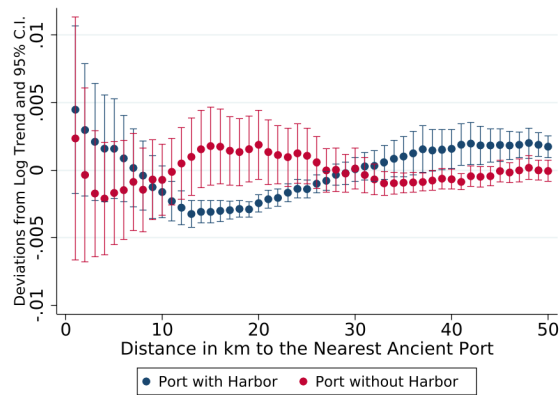
Panel A. Probability of City Density

Panel B. Probability of City Density

Panel C. Differences for City Density

Panel D. City, Difference from Log Fit

Notes: This figure reproduces estimates from Figures 6 and 7, instead using Conley standard errors (Conley, 1999) that allow for spatial correlation that declines linearly in distance up to an 8km cutoff. By comparison, the median size city in our sample has a radius of 4km. Panels A and B correspond to Figure 6, Panels B and D. Panels B and D correspond to Figure 7, Panels B and D.